Numerical analysis of a uniform flow of a rarefied gas past a sphere on the basis of the Boltzmann equation for hard-sphere molecules

Shigeru Takata, Yoshio Sone, and Kazuo Aoki

京大・工　高田　滋　曽根　良夫　青木　一生

Department of Aeronautical Engineering, Kyoto University,
Kyoto 606-01, Japan

A slow uniform flow of a rarefied gas past a sphere is investigated on the basis of the linearized Boltzmann equation for hard-sphere molecules and the diffuse reflection condition. With the aid of a similarity solution, the Boltzmann equation is reduced to two simultaneous integro-differential equations with three independent variables, which are solved numerically. The collision integral is computed efficiently by the use of a numerical collision kernel [Phys. Fluids A 1, 363 (1989)]. The velocity distribution function of the gas molecules, which has discontinuity in the gas, the density, flow velocity, and temperature fields of the gas, and the drag on the sphere are obtained accurately for the whole range of the Knudsen number. In spite of slow flow, the temperature is nonuniform (thermal polarization). From the behavior of the velocity distribution function, the kinetic transition region is clearly seen to separate into the Knudsen layer and the S layer for small Knudsen numbers.

I.   INTRODUCTION

A slow uniform flow of a rarefied gas past a sphere, or motion of a very small particle in a gas, is one of the simplest and most fundamental problems in rarefied gas dynamics, and aerosol sciences, and has interested many scientists and engineers.[1-16] Millikan's experiments[1,3] are famous among the works on this subject. Cercignani et al.[8] analyzed the problem by their variational method[17] on the basis of the Boltzmann-Krook-Welander (BKW or BGK) equation[18,19] and obtained the drag on the sphere for the whole range of the Knudsen number.[20] Their results agree very well with recent more detailed computations although a very simple test function was used. The behavior of the gas around the sphere is studied in Refs. 10,11,12,14, and 15. In Refs. 10 and 15, the asymptotic behavior of the gas for small Knudsen numbers is obtained analytically up to the second order of the Knudsen number with the aid of the asymptotic theory[21,22] of the Boltzmann system. According to Refs. 10 and 15, in contrast to the solution of classical fluid dynamics, the temperature around the sphere is nonuniform even in a slow flow, which is called thermal polarization.[13] The explicit expression of the nonuniform temperature field is given in Ref. 15. In Refs. 12 and 14, Loyalka et al. carried out numerical computation of the simultaneous integral equations for macroscopic variables derived from the BKW equation and diffuse reflection condition. There is some discrepancy between the results of the temperature field in Refs. 14 and 15. The information obtained so far is for the BKW model equation, and very few have been done on this subject on the basis of the standard Boltzmann equation; recently, limited results on the drag have been reported in Refs. 23 and 24. In this paper we will carry out accurate and detailed numerical study of the problem on the basis of the Boltzmann equation for hard-sphere molecules and clarify the comprehensive behavior of the

flow field for the whole range of the Knudsen number. It is shown in Refs. 25 and 26 that the velocity distribution function of gas molecules has discontinuity in a gas around a convex body. The discontinuity not only is interesting to be investigated accurately but also should be treated carefully to obtain the accurate information of the macroscopic variables. From the behavior of the velocity distribution function, we will see separation of the kinetic transition region into the Knudsen layer and the S layer[26,27] for small Knudsen numbers (Sec. V C).

II.   PROBLEM AND PRELIMINARY ANALYSIS

A.   Problem and notations

Consider a uniform flow of a rarefied gas [velocity $(U_\infty, 0, 0)$, pressure p_∞, and temperature T_∞] past a spherical body (radius L and temperature T_∞) at rest. We will investigate the steady behavior of the gas under the following assumptions: (i) The gas molecules are hard spheres of a uniform size and undergo complete elastic collision between themselves; (ii) The gas molecules are reflected diffusely on the sphere; and (iii) The flow speed (U_∞) is so small compared with the speed of the sound that the basic equation (the Boltzmann equation for hard-sphere molecules) and the boundary condition can be linearized around a uniform equilibrium state at rest.

We summarize the main notations used in this paper: $\rho_\infty = p_\infty/RT_\infty$; R is the specific gas constant (the Boltzmann constant divided by the mass of the molecule); l_∞ is the mean free path of the gas molecules at the equilibrium state at rest with pressure p_∞ and temperature T_∞ [for a hard-sphere molecular gas, $l_\infty = (\sqrt{2}\pi\sigma^2\rho_\infty/m)^{-1}$, where σ and m are the diameter and mass of the molecule, respectively]; Kn $= l_\infty/L$ (Knudsen number); $k_\infty = \pi^{1/2}\text{Kn}/2$; Lx_i is the Cartesian coordinate system with its origin at the center of the sphere and with its x_1 axis in the direction of the uniform flow; (rL, θ, φ) is the polar coordinate system with $r = 0$ at the center of the sphere and with $\theta = 0$ (the polar direction) in the x_1 direction; $(2RT_\infty)^{1/2}\zeta_i$ is the molecular velocity; $\zeta = |\zeta_i| = (\zeta_i^2)^{1/2}$; ζ_r, ζ_θ, and ζ_φ are, respectively, the r, θ, and φ components of ζ_i in the polar coordinate system; $E(\zeta) = \pi^{-3/2}\exp(-\zeta^2)$; $\rho_\infty(2RT_\infty)^{-3/2}E(1 + \phi)$ is the velocity distribution function of the gas molecules; $\rho_\infty(1 + \omega)$ is the density of the gas; $T_\infty(1 + \tau)$ is the temperature; $p_\infty(1 + P)$ is the pressure; $(2RT_\infty)^{1/2}u_i$ is the flow velocity; $p_\infty(\delta_{ij} + P_{ij})$ is the stress tensor; and $p_\infty(2RT_\infty)^{1/2}Q_i$ is the heat flow vector, where δ_{ij} is Kronecker's delta. The components of u_i, P_{ij}, and, Q_i in (r, θ, φ) system are expressed by the subscripts r, θ, and φ (e.g., u_r, u_θ). (See Fig. 1.)

B.   Basic equation and boundary condition

The linearized Boltzmann equation for a steady state is written as:

$$\zeta_i \frac{\partial \phi}{\partial x_i} = \frac{1}{k_\infty}\mathcal{L}(\phi). \tag{1}$$

For a hard-sphere molecular gas, the linearized collision integral $\mathcal{L}(\phi)$ is expressed in the following form:[28,29]

$$\mathcal{L}(\phi) = \mathcal{L}_1(\phi) - \mathcal{L}_2(\phi) - \nu(\zeta)\phi, \tag{2}$$

$$\mathcal{L}_1(\phi) = \frac{1}{\sqrt{2}\pi} \int \frac{1}{|\zeta_i - \xi_i|} \exp\left(-\xi_j^2 + \frac{(\varepsilon_{ijk}\zeta_j\xi_k)^2}{(\zeta_h - \xi_h)^2}\right) \phi(x_i, \xi_i)d\xi_1 d\xi_2 d\xi_3, \tag{3a}$$

$$\mathcal{L}_2(\phi) = \frac{1}{2\sqrt{2}\pi} \int |\zeta_i - \xi_i| \exp(-\xi_j^2)\phi(x_i, \xi_i)d\xi_1 d\xi_2 d\xi_3, \tag{3b}$$

$$\nu(\zeta) = \frac{1}{2\sqrt{2}} \left[\exp(-\zeta^2) + (2\zeta + \frac{1}{\zeta}) \int_0^\zeta \exp(-\xi^2) d\xi \right]. \tag{3c}$$

Here ε_{ijk} is Eddington's epsilon (thus, $\varepsilon_{ijk}\zeta_j\xi_k$ is the vector product of ζ_i and ξ_i); and the domain of integration in $\mathcal{L}_1$, $\mathcal{L}_2$, and all the following integrals with respect to the molecular velocity (ζ_i or ξ_i) is the whole molecular velocity space unless otherwise stated.

The (nondimensional) macroscopic variables ω, u_i, τ, etc. are given by the moments of ϕ:

$$\omega = \int \phi E \, d\zeta_1 \, d\zeta_2 \, d\zeta_3, \tag{4a}$$

$$u_i = \int \zeta_i \phi E \, d\zeta_1 \, d\zeta_2 \, d\zeta_3, \tag{4b}$$

$$\tau = \frac{2}{3} \int (\zeta_j^2 - \frac{3}{2}) \phi E \, d\zeta_1 \, d\zeta_2 \, d\zeta_3, \tag{4c}$$

$$P = \omega + \tau, \tag{4d}$$

$$P_{ij} = 2 \int \zeta_i \zeta_j \phi E \, d\zeta_1 \, d\zeta_2 \, d\zeta_3, \tag{4e}$$

$$Q_i = \int \zeta_i(\zeta_j^2 - \frac{5}{2}) \phi E \, d\zeta_1 \, d\zeta_2 \, d\zeta_3. \tag{4f}$$

The linearized form of the diffuse reflection boundary condition on the sphere ($x_i^2 = 1$) at rest and with temperature T_∞ is given by

$$\phi(x_i, \zeta_i) = \sigma_w, \qquad (\zeta_i n_i > 0), \tag{5}$$

$$\sigma_w = -2\pi^{1/2} \int_{\xi_i n_i < 0} \xi_j n_j \phi E \, d\xi_1 \, d\xi_2 \, d\xi_3, \tag{6}$$

where n_i is the unit normal vector to the boundary, pointed to the gas. The boundary condition at infinity [uniform equilibrium flow with pressure p_∞, temperature T_∞, and velocity $(U_\infty, 0, 0)$] is given as

$$\phi = 2\zeta_1 u_\infty, \tag{7}$$

with

$$u_\infty = U_\infty (2RT_\infty)^{-1/2}. \tag{8}$$

C. Similarity solution

According to Ref. 30, the solution of the boundary-value problem, Eqs. (1), (5), and (7), can be expressed by the following similarity solution:

$$\phi = \Phi_c(r, \zeta, \theta_\zeta) \cos\theta + \zeta_\theta \Phi_s(r, \zeta, \theta_\zeta) \sin\theta, \tag{9}$$

$$\theta_\zeta = \pi - \text{Arccos}(\zeta_r/\zeta), \qquad (0 \le \theta_\zeta \le \pi). \tag{10}$$

The $\pi - \theta_\zeta$ is the angle between the molecular velocity ζ_i and the radial direction. Then Φ_c and Φ_s are determined by the following equations:

$$\mathcal{D}\Phi_c + \frac{(\zeta \sin\theta_\zeta)^2}{r} \Phi_s = \frac{1}{k_\infty} \left[\mathcal{L}_1^c(\Phi_c) - \mathcal{L}_2^c(\Phi_c) - \nu(\zeta)\Phi_c \right], \tag{11}$$

$$\mathcal{D}(\Phi_s \zeta \sin\theta_\zeta) - \frac{\zeta \sin\theta_\zeta}{r} \Phi_c = \frac{1}{k_\infty} \left[\mathcal{L}_1^s(\Phi_s \zeta \sin\theta_\zeta) - \mathcal{L}_2^s(\Phi_s \zeta \sin\theta_\zeta) - \nu(\zeta)\Phi_s \zeta \sin\theta_\zeta \right], \tag{12}$$

where

$$\mathcal{D}\Phi = -\zeta \cos \theta_\zeta \frac{\partial \Phi}{\partial r} + \frac{\zeta \sin \theta_\zeta}{r} \frac{\partial \Phi}{\partial \theta_\zeta}, \tag{13}$$

$$\mathcal{L}_1^c(\Phi) = \frac{1}{\sqrt{2\pi}} \int_0^\infty \int_0^\pi \int_0^{2\pi} \frac{\xi^2 \sin \theta_\xi}{\mathcal{F}_1} \exp\left(-\xi^2 + \frac{\mathcal{F}_2}{\mathcal{F}_1^2}\right) \Phi(r, \xi, \theta_\xi)\, d\bar{\psi}\, d\theta_\xi\, d\xi, \tag{14a}$$

$$\mathcal{L}_2^c(\Phi) = \frac{1}{2\sqrt{2\pi}} \int_0^\infty \int_0^\pi \int_0^{2\pi} \mathcal{F}_1 \xi^2 \sin \theta_\xi \exp(-\xi^2) \Phi(r, \xi, \theta_\xi)\, d\bar{\psi}\, d\theta_\xi\, d\xi, \tag{14b}$$

$$\mathcal{L}_1^s(\Phi) = \frac{1}{\sqrt{2\pi}} \int_0^\infty \int_0^\pi \int_0^{2\pi} \frac{\xi^2 \sin \theta_\xi \cos \bar{\psi}}{\mathcal{F}_1} \exp\left(-\xi^2 + \frac{\mathcal{F}_2}{\mathcal{F}_1^2}\right) \Phi(r, \xi, \theta_\xi)\, d\bar{\psi}\, d\theta_\xi\, d\xi, \tag{15a}$$

$$\mathcal{L}_2^s(\Phi) = \frac{1}{2\sqrt{2\pi}} \int_0^\infty \int_0^\pi \int_0^{2\pi} \mathcal{F}_1 \xi^2 \sin \theta_\xi \cos \bar{\psi} \exp(-\xi^2) \Phi(r, \xi, \theta_\xi)\, d\bar{\psi}\, d\theta_\xi\, d\xi, \tag{15b}$$

$$\mathcal{F}_1 = \left[\zeta^2 + \xi^2 - 2\zeta\xi(\cos \theta_\zeta \cos \theta_\xi + \sin \theta_\zeta \sin \theta_\xi \cos \bar{\psi})\right]^{1/2}, \tag{16a}$$

$$\mathcal{F}_2 = \zeta^2 \xi^2 \left[\cos^2 \theta_\zeta \sin^2 \theta_\xi + \sin^2 \theta_\zeta \cos^2 \theta_\xi + \sin^2 \theta_\zeta \sin^2 \theta_\xi \sin^2 \bar{\psi}\right.$$
$$\left. - 2 \cos \theta_\zeta \sin \theta_\zeta \cos \theta_\xi \sin \theta_\xi \cos \bar{\psi}\right]. \tag{16b}$$

The set $(\xi,\, \pi - \theta_\xi,\, \bar{\psi})$ corresponds to the polar coordinate expression of ξ_i in Eqs. (3a) and (3b), with the polar direction in the radial direction.

The boundary conditions for Φ_c and Φ_s are:

at $r = 1$,

$$\left.\begin{array}{rcl} \Phi_c & = & 2\pi^{3/2} \displaystyle\int_0^\infty \int_0^{\pi/2} \zeta^3 \sin 2\theta_\zeta \Phi_c E\, d\theta_\zeta\, d\zeta, \\[4mm] \Phi_s & = & 0, \end{array}\right\} \quad (\pi/2 < \theta_\zeta \le \pi), \tag{17}$$

and as $r \to \infty$,

$$\left.\begin{array}{rcl} \Phi_c & \to & -2\zeta \cos \theta_\zeta u_\infty, \\[4mm] \Phi_s & \to & -2u_\infty. \end{array}\right\} \tag{18}$$

The boundary-value problem, Eqs. (1), (5), and (7), for a single integro-differential equation of six independent variables is reduced to that, Eqs. (11), (12), (17), and (18), for two simultaneous integro-differential equations of three independent variables, which will be analyzed numerically in the next section.

The macroscopic variables ω, u_r, u_θ, etc. are expressed by Φ_c and Φ_s as follows:

$$\omega = 2\pi \left(\int_0^\infty \int_0^\pi \zeta^2 \sin \theta_\zeta \Phi_c E\, d\theta_\zeta\, d\zeta\right) \cos \theta, \tag{19a}$$

$$u_r = -\pi \left(\int_0^\infty \int_0^\pi \zeta^3 \sin 2\theta_\zeta \Phi_c E\, d\theta_\zeta\, d\zeta\right) \cos \theta, \tag{19b}$$

$$u_\theta = \pi \left(\int_0^\infty \int_0^\pi \zeta^4 \sin^3 \theta_\zeta \Phi_s E\, d\theta_\zeta\, d\zeta\right) \sin \theta, \tag{19c}$$

$$u_\varphi = 0, \tag{19d}$$

$$\tau = \frac{4}{3}\pi \left[\int_0^\infty \int_0^\pi \zeta^2\left(\zeta^2 - \frac{3}{2}\right) \sin \theta_\zeta \Phi_c E\, d\theta_\zeta\, d\zeta\right] \cos \theta, \tag{19e}$$

$$P_{rr} = 4\pi \left(\int_0^\infty \int_0^\pi \zeta^4 \cos^2 \theta_\zeta \sin \theta_\zeta \Phi_c E\, d\theta_\zeta\, d\zeta \right) \cos \theta, \tag{19f}$$

$$P_{\theta\theta} = 2\pi \left(\int_0^\infty \int_0^\pi \zeta^4 \sin^3 \theta_\zeta \Phi_c E\, d\theta_\zeta\, d\zeta \right) \cos \theta, \tag{19g}$$

$$P_{r\theta} = -2\pi \left(\int_0^\infty \int_0^\pi \zeta^5 \cos \theta_\zeta \sin^3 \theta_\zeta \Phi_s E\, d\theta_\zeta\, d\zeta \right) \sin \theta, \tag{19h}$$

$$P_{\varphi\varphi} = 3(\omega + \tau) - P_{rr} - P_{\theta\theta}, \qquad P_{r\varphi} = P_{\theta\varphi} = 0, \tag{19i}$$

$$Q_r = -\pi \left[\int_0^\infty \int_0^\pi \zeta^3 (\zeta^2 - \frac{5}{2}) \sin 2\theta_\zeta \Phi_c E\, d\theta_\zeta\, d\zeta \right] \cos \theta, \tag{19j}$$

$$Q_\theta = \pi \left[\int_0^\infty \int_0^\pi \zeta^4 (\zeta^2 - \frac{5}{2}) \sin^3 \theta_\zeta \Phi_s E\, d\theta_\zeta\, d\zeta \right] \sin \theta, \tag{19k}$$

$$Q_\varphi = 0. \tag{19l}$$

D. Discontinuity of the velocity distribution function

The Boltzmann equation (1) defines the variation of ϕ in the direction of ζ_i in the x_i space. If there is a discontinuity of ϕ at $x_i = x_i^{(0)}$ and $\zeta_i = \zeta_i^{(0)}$, it propagates along the characteristic $x_i = x_i^{(0)} + \zeta_i^{(0)} t$, where $t\ (> 0)$ is a parameter. Since the $\mathcal{L}_1$ and $\mathcal{L}_2$ terms of the collision integral $\mathcal{L}(\phi)$ are continuous, the variation of the discontinuity is determined by

$$\zeta_i \frac{\partial [\phi]}{\partial x_i} = -\frac{1}{k_\infty} \nu(\zeta)[\phi], \tag{20}$$

where $[\phi]$ is the difference of ϕ on both sides of the discontinuity. The discontinuity decays in the length scale of the free path of the molecule with velocity ζ_i. The position of discontinuity is independent of molecular speed.

On a boundary the velocity distribution function of the molecules leaving the boundary is specified. That is

$$\phi = \sigma_w, \qquad (\zeta_i n_i > 0). \tag{21}$$

The feature of σ_w is quite different from ϕ with $\zeta_i n_i < 0$, which is established by collisions of surrounding gas molecules. Thus, ϕ on the boundary is generally discontinuous at $\zeta_i n_i = 0$. When the boundary is convex, this discontinuity propagates into the gas along the characteristic of Eq. (1). When the boundary is concave, on the other hand, the characteristic, which is tangent to the boundary, does not enter into the gas and therefore no discontinuity propagates into the gas. Thus at a given point x_i in the gas, ϕ is discontinuous at ζ_i whose opposite vector $(-\zeta_i)$ lies on the circular cone along which the edge of the sphere is viewed from x_i (Fig. 2).

By transformation into (r, ζ, θ_ζ) space or directly from the characteristics of Eqs. (11) and (12), the discontinuity of Φ_c and Φ_s in (r, ζ, θ_ζ) space is found to lie on the common surface:

$$r \sin \theta_\zeta = 1, \qquad (\pi/2 \leq \theta_\zeta \leq \pi). \tag{22}$$

In the following numerical analysis of Φ_c and Φ_s, the difference formulae of differentiation that contain the data on both sides of the discontinuity should be avoided.

More about the discontinuity of the velocity distribution function, especially its relation to the S layer[27] at the bottom of the Knudsen layer, are found in Refs. 25, 26 and 31.

III. ASYMPTOTIC SOLUTIONS FOR LARGE AND SMALL KNUDSEN NUMBERS

Before proceeding to numerical analysis of the problem, we give the asymptotic solution of the boundary-value problem, Eqs. (11), (12), (17), and (18), for two limiting cases $k_\infty \to \infty$ and $k_\infty \to 0$.

For the free molecular limit ($k_\infty = \infty$), where the collision term of the Boltzmann equation is neglected, the solution is obtained as follows:

$$\frac{\Phi_c}{u_\infty} = \begin{cases} -2\zeta \cos\theta_\zeta, & [0 \le \theta_\zeta < \pi - \text{Arcsin}(\frac{1}{r})], \\ \sqrt{\pi} \left[\cos\theta_\zeta (1 - r^2 \sin^2\theta_\zeta)^{1/2} - r \sin^2\theta_\zeta \right], & [\pi - \text{Arcsin}(\frac{1}{r}) < \theta_\zeta \le \pi], \end{cases} \tag{23}$$

$$\frac{\Phi_s}{u_\infty} = \begin{cases} -2, & [0 \le \theta_\zeta < \pi - \text{Arcsin}(\frac{1}{r})], \\ \sqrt{\pi}\zeta^{-1} \left[r \cos\theta_\zeta + (1 - r^2 \sin^2\theta_\zeta)^{1/2} \right], & [\pi - \text{Arcsin}(\frac{1}{r}) < \theta_\zeta \le \pi], \end{cases} \tag{24}$$

$$\frac{\omega}{u_\infty \cos\theta} = -\frac{\sqrt{\pi}}{6}\left\{ (1 + \frac{6}{\pi})r^{-2} + \left[2 - (2 + r^{-2})(1 - r^{-2})^{1/2} \right] r \right\}, \tag{25a}$$

$$\frac{u_r}{u_\infty \cos\theta} = \frac{1}{2} + \frac{1}{2}(1 - r^{-2})^{3/2} - \frac{1}{4}r^{-3} - \int_0^{1/r} t(1 - t^2)^{1/2}(1 - r^2 t^2)^{1/2} dt, \tag{25b}$$

$$\frac{u_\theta}{u_\infty \sin\theta} = -\frac{1}{2} - \frac{1}{4}(1 - r^{-2})^{1/2}(2 + r^{-2}) - \frac{1}{8}r^{-3}$$

$$+ \frac{1}{2}\int_0^{1/r} t^3(1 - t^2)^{-1/2}(1 - r^2 t^2)^{1/2} dt, \tag{25c}$$

$$\frac{\tau}{u_\infty \cos\theta} = -\frac{1}{3\sqrt{\pi}}r^{-2}. \tag{25d}$$

The asymptotic solution for small k_∞ [up to $O(k_\infty)$] is easily obtained with the aid of the asymptotic theory in Refs. 26, 31, 32 and 33 as follows:

$$\frac{\omega}{u_\infty \cos\theta} = -\frac{3}{2}\gamma_1 k_\infty r^{-2}, \tag{26a}$$

$$\frac{u_r}{u_\infty \cos\theta} = 1 - \frac{3}{2}(1 + \kappa_0 k_\infty)r^{-1} + \frac{1}{2}(1 + 3\kappa_0 k_\infty)r^{-3}, \tag{26b}$$

$$\frac{u_\theta}{u_\infty \sin\theta} = -1 + \frac{3}{4}(1 + \kappa_0 k_\infty)r^{-1} + \frac{1}{4}(1 + 3\kappa_0 k_\infty)r^{-3} + \frac{3}{2}k_\infty Y_0(\eta), \tag{26c}$$

$$\tau = 0, \tag{26d}$$

where γ_1, κ_0, and $Y_0(\eta)$ are determined by the molecular model. That is,

$$\left. \begin{array}{lll} \gamma_1 = 1.270042, & \kappa_0 = -1.2540, & \text{(hard-sphere molecules)}, \\ \\ \gamma_1 = 1, & \kappa_0 = -1.01619, & \text{(BKW model)}, \end{array} \right\} \tag{27}$$

and $Y_0(\eta)$, called Knudsen-layer function for the shear flow, is a function of the stretched coordinate η defined by $\eta = (r - 1)/k_\infty$ and tabulated in Ref. 34 for hard-sphere molecules and

in Ref. 35 for the BKW model ($[Y_0(\eta), \eta]$ (here, Refs. 26, 32, 33) $= [-S(x_1), x_1]$ (Ref. 34)). The constants γ_1 and κ_0 are related to the viscosity and the slip coefficient of the shear flow, respectively [Refs. 26, 31, etc.; $\kappa_0 = -\beta_A$ (Ref. 34)]. The pressure is obtained up to $O(k_\infty^2)$, except for the Knudsen-layer correction, as

$$\frac{P}{u_\infty \cos\theta} = -\frac{3}{2}\gamma_1 k_\infty (1 + \kappa_0 k_\infty) r^{-2}. \tag{28}$$

IV. METHOD OF NUMERICAL ANALYSIS

A. Process of numerical computation by a finite difference method

In the present paper we analyze the boundary-value problem, Eqs. (11), (12), (17), and (18), numerically by a finite difference method. As is pointed out in Sec. II D, the velocity distribution functions Φ_c and Φ_s are discontinuous along $r\sin\theta_\zeta = 1$ ($\pi/2 \le \theta_\zeta \le \pi$). In order to describe the discontinuity accurately and avoid errors owing to it, a special care is required in constructing the difference scheme.[25] The problem is considered over a finite domain ($1 \le r \le r_D$, $0 \le \zeta \le \zeta_D$, $0 \le \theta_\zeta \le \pi$), where r_D and ζ_D are chosen properly depending on situations. The process of reduction to the finite domain will be discussed in Sec. IV C. Let ($r^{(i)}, \zeta^{(j)}, \theta_\zeta^{(k)}$) be the lattice points in the domain, where $i = 0, 1, \ldots, I$ ($r^{(0)} = 1$, $r^{(I)} = r_D$), $j = 0, 1, \ldots, J$ ($\zeta^{(0)} = 0$, $\zeta^{(J)} = \zeta_D$), and $k = 0, 1, \ldots, \widehat{K}, \ldots, K$ ($\theta_\zeta^{(0)} = 0$, $\theta_\zeta^{(\widehat{K})} = \pi/2$, $\theta_\zeta^{(K)} = \pi$). The functions $\Phi(r, \zeta, \theta_\zeta)$ of (r, ζ, θ_ζ), $f(r)$ of r, etc. at a lattice point are denoted by the subscripts corresponding to the lattice point:

$$\Phi_{(i,j,k)} = \Phi(r^{(i)}, \zeta^{(j)}, \theta_\zeta^{(k)}), \qquad f_{(i)} = f(r^{(i)}). \tag{29}$$

In the followings we introduce a new function $\widehat{\Phi}_s$ defined by

$$\widehat{\Phi}_s = \Phi_s \zeta \sin\theta_\zeta, \tag{30}$$

and carry out analysis in terms of Φ_c and $\widehat{\Phi}_s$ instead of Φ_c and Φ_s. We construct the discrete solutions $\Phi_{c(i,j,k)}$ and $\widehat{\Phi}_{s(i,j,k)}$ of Eqs. (11), (12), (17), and (18) as the limit of the sequences $\Phi_{c(i,j,k)}^{(n)}$ and $\widehat{\Phi}_{s(i,j,k)}^{(n)}$ ($n = 0, 1, 2, \ldots$) obtained by the iteration process described below.

Corresponding to Eqs. (11) and (12), the following finite difference equations for $\Phi_{c(i,j,k)}^{(n)}$ and $\widehat{\Phi}_{s(i,j,k)}^{(n)}$ are adopted:

$$-\zeta^{(j)} \cos\theta_\zeta^{(k)} \nabla_1^{(i,j,k)} \Phi_c^{(n)} + \frac{\zeta^{(j)} \sin\theta_\zeta^{(k)}}{r^{(i)}} \nabla_2^{(i,j,k)} \Phi_c^{(n)} + \frac{\zeta^{(j)} \sin\theta_\zeta^{(k)}}{r^{(i)}} \widehat{\Phi}_{s(i,j,k)}^{(n)}$$
$$= \frac{1}{k_\infty} \left(C_{(i,j,k)}^{(n-1)} - \nu_{(j)} \Phi_{c(i,j,k)}^{(n)} \right), \tag{31}$$

$$-\zeta^{(j)} \cos\theta_\zeta^{(k)} \nabla_1^{(i,j,k)} \widehat{\Phi}_s^{(n)} + \frac{\zeta^{(j)} \sin\theta_\zeta^{(k)}}{r^{(i)}} \nabla_2^{(i,j,k)} \widehat{\Phi}_s^{(n)} - \frac{\zeta^{(j)} \sin\theta_\zeta^{(k)}}{r^{(i)}} \Phi_{c(i,j,k)}^{(n)}$$
$$= \frac{1}{k_\infty} \left(\widehat{S}_{(i,j,k)}^{(n-1)} - \nu_{(j)} \widehat{\Phi}_{s(i,j,k)}^{(n)} \right), \tag{32}$$

where $\nabla_1^{(i,j,k)}$ and $\nabla_2^{(i,j,k)}$ correspond to $\partial/\partial r$ and $\partial/\partial\theta_\zeta$ operators, respectively, given explicitly below, and $C_{(i,j,k)}^{(n)}$ and $\widehat{S}_{(i,j,k)}^{(n)}$ are the collision integrals:

$$C_{(i,j,k)}^{(n)} = \left[\mathcal{L}_1^c(\Phi_c^{(n)}) - \mathcal{L}_2^c(\Phi_c^{(n)})\right]_{(i,j,k)} , \tag{33}$$

$$\widehat{S}_{(i,j,k)}^{(n)} = \left[\mathcal{L}_1^s(\widehat{\Phi}_s^{(n)}) - \mathcal{L}_2^s(\widehat{\Phi}_s^{(n)})\right]_{(i,j,k)} . \tag{34}$$

An efficient way of computation of $C_{(i,j,k)}^{(n)}$ and $\widehat{S}_{(i,j,k)}^{(n)}$, adopted in the paper, is given in the next subsection (Sec. IV B).

We use the following formulae for the ∇_1 and ∇_2 operators:

$$\nabla_1^{(i,j,k)}\Phi = \begin{cases} [-(\Lambda_{(i+1)} + 2)\Phi_{(i,j,k)} + (\Lambda_{(i+1)} + \Lambda_{(i+1)}^{-1} + 2)\Phi_{(i+1,j,k)} \\ \qquad -\Lambda_{(i+1)}^{-1}\Phi_{(i+2,j,k)}]/(\Delta r^{(i+1)} + \Delta r^{(i+2)}), \\ \qquad\qquad\qquad\qquad (0 \le i \le I - 2, \ 0 \le k \le \widehat{K}), \\ (\Phi_{(1,j,k)} - \Phi_{(0,j,k)})/\Delta r^{(1)}, \qquad (i = 1, \ \widehat{K} + 1 \le k \le K), \\ [(\Lambda_{(i-1)}^{-1} + 2)\Phi_{(i,j,k)} - (\Lambda_{(i-1)} + \Lambda_{(i-1)}^{-1} + 2)\Phi_{(i-1,j,k)} \\ \qquad +\Lambda_{(i-1)}\Phi_{(i-2,j,k)}]/(\Delta r^{(i-1)} + \Delta r^{(i)}), \\ \qquad\qquad\qquad\qquad (2 \le i \le I, \ \widehat{K} + 1 \le k \le K), \end{cases} \tag{35a}$$

$$\nabla_2^{(i,j,k)}\Phi = \begin{cases} (\Phi_{(i,j,1)} - \Phi_{(i,j,0)})/\Delta\theta_\zeta^{(1)}, \qquad\qquad (k = 1), \\ [(\lambda_{(k-1)}^{-1} + 2)\Phi_{(i,j,k)} - (\lambda_{(k-1)} + \lambda_{(k-1)}^{-1} + 2)\Phi_{(i,j,k-1)} \\ \qquad +\lambda_{(k-1)}\Phi_{(i,j,k-2)}]/(\Delta\theta_\zeta^{(k-1)} + \Delta\theta_\zeta^{(k)}), \qquad (2 \le k \le K), \end{cases} \tag{35b}$$

$$\left.\begin{array}{cc} \Delta r^{(i)} = r^{(i)} - r^{(i-1)}, & \Delta\theta_\zeta^{(k)} = \theta_\zeta^{(k)} - \theta_\zeta^{(k-1)}, \\ \Lambda_{(i)} = \dfrac{\Delta r^{(i+1)}}{\Delta r^{(i)}}, & \lambda_{(k)} = \dfrac{\Delta\theta_\zeta^{(k+1)}}{\Delta\theta_\zeta^{(k)}}. \end{array}\right\} \tag{35c}$$

As explained in Sec. II D, Φ_c and $\widehat{\Phi}_s$ are discontinuous along $r\sin\theta_\zeta = 1$ $(\pi/2 \le \theta_\zeta \le \pi)$. The difference formulae (35a) and (35b) should be modified when they consist of the data on both sides of the discontinuity. That is,

$$\nabla_1^{(i,j,k)}\Phi = \begin{cases} A_1\Phi_{(i,j,k)} - A_2\Phi_{(i-1,j,k)} + A_3\Phi_{(i(k),j,k)+}, & (r^{(i-1)} > 1/\sin\theta_\zeta^{(k)} \ge r^{(i-2)}), \\ (\Phi_{(i,j,k)} - \Phi_{(i(k),j,k)+})/(r^{(i)} - 1/\sin\theta_\zeta^{(k)}), & (r^{(i)} > 1/\sin\theta_\zeta^{(k)} \ge r^{(i-1)}), \end{cases} \tag{36a}$$

$$\nabla_2^{(i,j,k)}\Phi = \begin{cases} B_1\Phi_{(i,j,k)} - B_2\Phi_{(i,j,k-1)} + B_3\Phi_{(i,j,k(i))-}, \\[4pt] \qquad\qquad [\theta_\zeta^{(k-1)} > \pi - \text{Arcsin}(1/r^{(i)}) \geq \theta_\zeta^{(k-2)}], \\[8pt] (\Phi_{(i,j,k)} - \Phi_{(i,j,k(i))})-)/[\theta_\zeta^{(k)} + \text{Arcsin}(1/r^{(i)}) - \pi], \\[4pt] \qquad\qquad [\theta_\zeta^{(k)} > \pi - \text{Arcsin}(1/r^{(i)}) \geq \theta_\zeta^{(k-1)}], \end{cases} \tag{36b}$$

where

$$\Phi_{(i(k),j,k)\pm} = \Phi(1/\sin\theta_\zeta^{(k)} \pm 0, \zeta^{(j)}, \theta_\zeta^{(k)}), \tag{37a}$$

$$\Phi_{(i,j,k(i))\pm} = \Phi(r^{(i)}, \zeta^{(j)}, \pi - \text{Arcsin}(1/r^{(i)}) \mp 0), \tag{37b}$$

and A_1, A_2, and A_3 (B_1, B_2, and B_3) are chosen in such a way that $\nabla_1^{(i,j,k)}\Phi$ ($\nabla_2^{(i,j,k)}\Phi$) is the difference expression of the second-order accuracy for $\partial\Phi/\partial r$ ($\partial\Phi/\partial\theta_\zeta$) at $(r^{(i)}, \zeta^{(j)}, \theta_\zeta^{(k)})$. A_1, A_2, A_3, B_1, B_2, and B_3 depend only on i and k. It is noted that $(i(k), j, k)$ and $(i, j, k(i))$ are not regular lattice points. The $i(k)$ and $k(i)$ represent the intersection of the characteristic $r\sin\theta_\zeta = 1$ with the lattice lines $\theta_\zeta = \theta_\zeta^{(k)}$ and $r = r^{(i)}$ respectively. That is

$$\left. \begin{array}{rcl} r^{(i(k))} &=& 1/\sin\theta_\zeta^{(k)}, \\[8pt] \theta^{(k(i))} &=& \pi - \text{Arcsin}(1/r^{(i)}). \end{array} \right\} \tag{38}$$

When a discontinuous function on the characteristic is considered, the two limiting cases as in Eqs. (37a) and (37b) should be considered. The formulae contain $\Phi_{(i(k),j,k)+}$ and $\Phi_{(i,j,k(i))-}$, i.e., Φ on either side of the discontinuity. The sequences $\Phi_{c(i,j,k(i))\pm}^{(n)}$ and $\widehat{\Phi}_{s(i,j,k(i))\pm}^{(n)}$, corresponding to Φ_c and $\widehat{\Phi}_s$ at $r^{(i)}$ on either side of the discontinuity, are constructed by the following difference scheme:

$$-\zeta^{(j)}\cos\theta_\zeta^{(k(i))}\nabla_1^{(i,j)\pm}\Phi_c^{(n)} + \frac{\zeta^{(j)}\sin\theta_\zeta^{(k(i))}}{r^{(i)}}\widehat{\Phi}_{s(i,j,k(i))\pm}^{(n)}$$
$$= \frac{1}{k_\infty}\left(C_{(i,j,k(i))}^{(n-1)} - \nu_{(j)}\Phi_{c(i,j,k(i))\pm}^{(n)}\right), \tag{39}$$

$$-\zeta^{(j)}\cos\theta_\zeta^{(k(i))}\nabla_1^{(i,j)\pm}\widehat{\Phi}_s^{(n)} - \frac{\zeta^{(j)}\sin\theta_\zeta^{(k(i))}}{r^{(i)}}\Phi_{c(i,j,k(i))\pm}^{(n)}$$
$$= \frac{1}{k_\infty}\left(\widehat{S}_{(i,j,k(i))}^{(n-1)} - \nu_{(j)}\widehat{\Phi}_{s(i,j,k(i))\pm}^{(n)}\right), \tag{40}$$

where $\nabla_1^{(i,j)\pm}\Phi$ corresponds to $\nabla_1^{(i,j,k)}\Phi$ ($\widehat{K}+1 \leq k \leq K$) in Eq. (35a) with $\Phi_{(i,j,k)}$ replaced by $\Phi_{(i,j,k(i))\pm}$. The absence of $\pm$ sign in $C_{(i,j,k(i))}^{(n-1)}$ and $\widehat{S}_{(i,j,k(i))}^{(n-1)}$ corresponds to the fact that $\mathcal{L}_1(\phi)$ and $\mathcal{L}_2(\phi)$ are continuous.

The boundary conditions for $\Phi_{c(i,j,k)}^{(n)}$ and $\widehat{\Phi}_{s(i,j,k)}^{(n)}$ at $r = 1$ ($i = 0$) are obvious from Eq. (17). As the condition at $r = r_D$, instead of Eq. (18), we impose

$$\left. \begin{array}{rcl} \Phi_{c(I-1,j,k)}^{(n)} &=& G_{c(j,k)}^{(n)}, \\[8pt] \Phi_{c(I,j,k)}^{(n)} &=& H_{c(j,k)}^{(n)}, \end{array} \right\} \tag{41}$$

$$\begin{aligned}
\widehat{\Phi}^{(n)}_{s(I-1,j,k)} &= G^{(n)}_{s(j,k)} \ , \\
\widehat{\Phi}^{(n)}_{s(I,j,k)} &= H^{(n)}_{s(j,k)} \ ,
\end{aligned} \Bigg\}$$

(42)

where $G^{(n)}_{c(j,k)}$, $G^{(n)}_{s(j,k)}$, $H^{(n)}_{c(j,k)}$, and $H^{(n)}_{s(j,k)}$ are determined by the asymptotic solution for large r in Sec. IV C.

With these preparation of difference formulae, we construct the sequences $\Phi^{(n)}_{c(i,j,k)}$ and $\widehat{\Phi}^{(n)}_{s(i,j,k)}$ by the following process. Let $\Phi^{(n-1)}_{c(i,j,k)}$ and $\widehat{\Phi}^{(n-1)}_{s(i,j,k)}$ be known. Then $G^{(n)}_{c(j,k)}$, $G^{(n)}_{s(j,k)}$, $H^{(n)}_{c(j,k)}$, and $H^{(n)}_{s(j,k)}$ are known (Sec. IV C).

(i) For $0 \leq k \leq \widehat{K}$, starting from $\Phi^{(n)}_{c(I-2,j,k)}$ and $\widehat{\Phi}^{(n)}_{s(I-2,j,k)}$, compute $\Phi^{(n)}_{c(i,j,k)}$ and $\widehat{\Phi}^{(n)}_{s(i,j,k)}$ using Eqs. (31), (32), (41), and (42) in descending order of i down to $\Phi^{(n)}_{c(0,j,k)}$ and $\widehat{\Phi}^{(n)}_{s(0,j,k)}$. The step $i = i + 1$ to $i = i$ is as follows. Let $\Phi^{(n)}_{c(i',j,k)}$ and $\widehat{\Phi}^{(n)}_{s(i',j,k)}$ $(i' > i)$ be given. Starting from $\Phi^{(n)}_{c(i,j,0)}$ and $\widehat{\Phi}^{(n)}_{s(i,j,0)}$, compute $\Phi^{(n)}_{c(i,j,k)}$ and $\widehat{\Phi}^{(n)}_{s(i,j,k)}$ using Eqs. (31)-(35c) [and Eqs. (41) and (42) for $i = I-2, I-3$] in ascending order of k up to $\Phi^{(n)}_{c(i,j,\widehat{K})}$ and $\widehat{\Phi}^{(n)}_{s(i,j,\widehat{K})}$. Carry out this step for every j.

(ii) Compute $\Phi^{(n)}_{c(i,j,k(i))\pm}$ and $\widehat{\Phi}^{(n)}_{s(i,j,k(i))\pm}$ along the discontinuity using Eqs. (39) and (40): $\Phi^{(n)}_{c(i,j,k(i))+}$ and $\widehat{\Phi}^{(n)}_{s(i,j,k(i))+}$ are constructed from the initial data $\Phi^{(n)}_{c(0,j,\widehat{K})}$ and $\widehat{\Phi}^{(n)}_{s(0,j,\widehat{K})}$ obtained in the preceding step (i)[36]; $\Phi^{(n)}_{c(i,j,k(i))-}$ and $\widehat{\Phi}^{(n)}_{s(i,j,k(i))-}$ from the initial condition given by Eq. (17). The computation is continued until the discontinuity becomes negligibly small. Then, from a set of $\Phi^{(n)}_{c(i,j,k(i))+}$ $(\widehat{\Phi}^{(n)}_{s(i,j,k(i))+})$, obtain $\Phi^{(n)}_{c(i(k),j,k)+}$ $(\widehat{\Phi}^{(n)}_{s(i(k),j,k)+})$ by interpolation. [The data on the discontinuity in Eqs. (36a) and (36b) are now prepared.]

(iii) For $\widehat{K}+1 \leq k \leq K$, the computation is carried out in ascending order of i, independently in the two regions $r > 1/\sin\theta_\zeta$ and $r < 1/\sin\theta_\zeta$ separated by the discontinuity. The step $i = i - 1$ to $i = i$ is as follows. Let $\Phi^{(n)}_{c(i',j,k)}$ and $\widehat{\Phi}^{(n)}_{s(i',j,k)}$ $(i' < i)$ be given. (a) For $r > 1/\sin\theta_\zeta$, starting from $\Phi^{(n)}_{c(i,j,\widehat{K}+1)}$ and $\widehat{\Phi}^{(n)}_{s(i,j,\widehat{K}+1)}$, compute $\Phi^{(n)}_{c(i,j,k)}$ and $\widehat{\Phi}^{(n)}_{s(i,j,k)}$ using Eqs. (31), (32), (35a), (35b), (36a), and the data obtained in steps (i) and (ii) in ascending order of k up to $\Phi^{(n)}_{c(i,j,\bar{k})}$ and $\widehat{\Phi}^{(n)}_{s(i,j,\bar{k})}$, where $\theta_\zeta^{(\bar{k})} < \pi - \text{Arcsin}(1/r^{(i)}) \leq \theta_\zeta^{(\bar{k}+1)}$. (b) For $r < 1/\sin\theta_\zeta$, starting from $\Phi^{(n)}_{c(i,j,\bar{k}+1)}$ and $\widehat{\Phi}^{(n)}_{s(i,j,\bar{k}+1)}$, compute $\Phi^{(n)}_{c(i,j,k)}$ and $\widehat{\Phi}^{(n)}_{s(i,j,k)}$ using Eqs. (31), (32), (35a), (35b), (36b), the data of Eq. (17), and those obtained in step (ii) in ascending order of k up to $\Phi^{(n)}_{c(i,j,K)}$ and $\widehat{\Phi}^{(n)}_{s(i,j,K)}$. Carry out these steps for every j. For $i > i_c$, where the discontinuity is negligibly small, neglecting the discontinuity, compute $\Phi^{(n)}_{c(i,j,k)}$ and $\widehat{\Phi}^{(n)}_{s(i,j,k)}$ from $k = \widehat{K}+1$ to K only with the standard formulae (35a) and (35b) as in step (i).

(iv) Applying the Simpson formula to Eqs. (19b)-(19e), compute $(u_r/\cos\theta)^{(n)}_{(I)}$, $(u_\theta/\sin\theta)^{(n)}_{(I)}$, and $(\tau/\cos\theta)^{(n)}_{(I)}$. Then by the process of connection of these data to the asymptotic solution for large r (Sec. IV C), determine $G^{(n+1)}_{c(j,k)}$, $H^{(n+1)}_{c(j,k)}$, $G^{(n+1)}_{s(j,k)}$, and $H^{(n+1)}_{s(j,k)}$ in Eqs. (41) and (42).

(v) Repeat steps (i)-(iv) with shift of the superscript (n to $n+1$) until $\Phi^{(n)}_{c(i,j,k)}$ and $\widehat{\Phi}^{(n)}_{s(i,j,k)}$

converge. We take the limits as the solution ($\Phi_{c(i,j,k)}$ and $\widehat{\Phi}_{s(i,j,k)}$) of the problem, from which the macroscopic variables are obtained by integration [cf. Eqs. (19a)-(19l)].

The order of computation in the preceding process is consistent with the natural course of integration of Eqs. (11) and (12) along their characteristic in the direction of molecular velocity.

B.   Computation of collision integral

To compute the collision integrals $C_{(i,j,k)}^{(n)}$ and $\widehat{S}_{(i,j,k)}^{(n)}$ efficiently, which take the majority of the computing time, we make use of the numerical kernel method introduced in Ref. 37. That is, Φ_c and $\widehat{\Phi}_s$ at the nth step and $r = r^{(i)}$ are expanded in a set of basis functions:

$$\Phi_c^{(n)}(r^{(i)}, \zeta, \theta_\zeta) = \sum_{\ell,m} \Phi_{c(i,\ell,m)}^{(n)} \Psi_{\ell m}(\zeta, \theta_\zeta), \tag{43}$$

$$\widehat{\Phi}_s^{(n)}(r^{(i)}, \zeta, \theta_\zeta) = \sum_{\ell,m} \widehat{\Phi}_{s(i,\ell,m)}^{(n)} \Psi_{\ell m}(\zeta, \theta_\zeta), \tag{44}$$

where the basis functions $\Psi_{\ell m}(\zeta, \theta_\zeta)$ are chosen in such a way that $\Phi_c^{(n)}$ and $\widehat{\Phi}_s^{(n)}$ are continuous in ζ and θ_ζ, take $\Phi_{c(i,\ell,m)}^{(n)}$ and $\widehat{\Phi}_{s(i,\ell,m)}^{(n)}$, respectively, at the lattice points and are expressed by the quadratic functions of ζ and θ_ζ in each rectangle of 2×2 lattices with even lattice points at its four corners.[38] Then,

$$C_{(i,j,k)}^{(n)} = \sum_{\ell,m} \Phi_{c(i,\ell,m)}^{(n)} K_{jk\ell m}^c, \tag{45}$$

$$\widehat{S}_{(i,j,k)}^{(n)} = \sum_{\ell,m} \widehat{\Phi}_{s(i,\ell,m)}^{(n)} K_{jk\ell m}^s, \tag{46}$$

where $K_{jk\ell m}^c$ and $K_{jk\ell m}^s$ are, respectively, $C_{(i,j,k)}^{(n)}$ with $\Phi_c^{(n)} = \Psi_{\ell m}$ and $\widehat{S}_{(i,j,k)}^{(n)}$ with $\widehat{\Phi}_s^{(n)} = \Psi_{\ell m}$:

$$K_{jk\ell m}^c = [\mathcal{L}_1^c(\Psi_{\ell m}) - \mathcal{L}_2^c(\Psi_{\ell m})]_{(j,k)}, \tag{47}$$

$$K_{jk\ell m}^s = [\mathcal{L}_1^s(\Psi_{\ell m}) - \mathcal{L}_2^s(\Psi_{\ell m})]_{(j,k)}, \tag{48}$$

The $K_{jk\ell m}^c$ and $K_{jk\ell m}^s$ are universal constants, which can be computed beforehand and used in various problems. The computations of Eqs. (47) and (48), whose effective domain of integration is a slender ring with the support of $\Psi_{\ell m}$, where $\Psi_{\ell m} \neq 0$, as its cross section, should be carried out carefully since the kernels of Eqs. (14a) and (15a) have singularity.[39]

The discontinuities in $\zeta \theta_\zeta$ space of $\Phi_c^{(n)}(r^{(i)}, \zeta, \theta_\zeta)$ and $\widehat{\Phi}_s^{(n)}(r^{(i)}, \zeta, \theta_\zeta)$ cannot be described by the expansions (43) and (44). The expanded functions are inaccurate over a lattice elements in θ_ζ (say, $\theta_\zeta^{(2\kappa)} \leq \theta_\zeta < \theta_\zeta^{(2\kappa+2)}$, where κ depends on $r^{(i)}$) for all ζ. These local inaccuracies induce only negligible errors in the results (45) and (46) of integration over $\zeta \theta_\zeta$ space. In our computation, the discontinuity at $r^{(0)}$ (i.e. $r = 1$) is taken care of by introducing two limiting values [36] at $\theta_\zeta = \pi/2$ for $\Phi_{c(0,\ell,\widehat{K})}$ and $\widehat{\Phi}_{s(0,\ell,\widehat{K})}$. If the discontinuity happens to pass the lattice points $\theta_\zeta^{(k)}$ ($\widehat{k} = 2\kappa$ or $2\kappa + 1$), the limiting values $\Phi_c(r^{(i)}, \zeta^{(\ell)}, \theta_\zeta^{(k)} - 0)$ and $\widehat{\Phi}_s(r^{(i)}, \zeta^{(\ell)}, \theta_\zeta^{(k)} - 0)$ are taken as $\Phi_{c(i,\ell,\widehat{k})}$ and $\widehat{\Phi}_{s(i,\ell,\widehat{k})}$, respectively in Eqs. (45) and (46), and therefore the expanded functions are inaccurate over the lattice element $\theta_\zeta^{(2\kappa)} \leq \theta_\zeta < \theta_\zeta^{(2\kappa+2)}$.

C. Asymptotic behavior for large r and the condition at $r = r_D$

We have limited the original infinite domain to the finite one ($1 \le r \le r_D$, $0 \le \zeta \le \zeta_D$, $0 \le \theta_\zeta \le \pi$). It does not introduce any problem to limit the range of ζ. As is easily checked by computation, $\Phi_c E$ and $\Phi_s E$ decay very rapidly as $\zeta \to \infty$, and therefore the accurate computation of the problem can be carried out with a reasonable size of ζ_D. The problem is not so simple for the case of the r variable. From the asymptotic solutions for small k_∞ and $k_\infty = \infty$, the approach of ϕ (or Φ_c and Φ_s) to the uniform state at infinity is expected to be very slow ($\sim r^{-m}$). Thus, a very large r_D is required to obtain an accurate result by simple application of Eq. (7) at $r = r_D$. We therefore introduce a method to make use of the asymptotic solution for large r.

Let the deviation $\delta\phi (= \phi - 2\zeta_1 u_\infty)$ from the equilibrium state at infinity be $O(r^{-m})$ for large r, then $\partial \delta\phi/\partial r = r^{-1}O(\delta\phi)$. That is, for $r > r_A$ the characteristic length scale of variation of $\delta\phi$ is larger than r_A, and therefore the effective Knudsen number $\text{Kn}_{\text{eff}}(= \ell_\infty/L r_A = \text{Kn}/r_A)$ is small for large r_A. Thus, the asymptotic form of ϕ (or Φ_c and Φ_s) for large r is obtained with the aid of the asymptotic theory [21,22,32,33] for small Knudsen numbers as follows:

$$
\begin{aligned}
\frac{\Phi_c}{u_\infty} &= -2(1 + c_1 r^{-1} + c_2 r^{-3})\zeta \cos\theta_\zeta + c_3 r^{-2}(\zeta^2 - \frac{5}{2}) \\
&\quad + k_\infty r^{-2}[\gamma_1 c_1 - 2c_3 r^{-1}\zeta A(\zeta)\cos\theta_\zeta - \frac{1}{2}(c_1 + 3c_2 r^{-2})\zeta^2 B(\zeta)(1 - 3\cos^2\theta_\zeta)] \\
&\quad + k_\infty^2 r^{-3}\{2c_1\zeta D_1(\zeta)\cos\theta_\zeta + 3c_3 r^{-1}\zeta^2 F(\zeta)(1 - 3\cos^2\theta_\zeta) \\
&\quad - 2[c_1(3\cos^2\theta_\zeta - 2) + 3c_2 r^{-2}(5\cos^2\theta_\zeta - 3)]\zeta^3 D_2(\zeta)\cos\theta_\zeta\},
\end{aligned} \tag{49}
$$

$$
\begin{aligned}
\frac{\Phi_s}{u_\infty} &= -2 - c_1 r^{-1} + c_2 r^{-3} + k_\infty r^{-3}[c_3 A(\zeta) - 3c_2 r^{-1}\zeta B(\zeta)\cos\theta_\zeta] \\
&\quad + k_\infty^2 r^{-3}\{-c_1 D_1(\zeta) + 6c_3 r^{-1}\zeta F(\zeta)\cos\theta_\zeta \\
&\quad - \frac{1}{2}[c_1(1 - 3\cos^2\theta_\zeta) + 9c_2 r^{-2}(1 - 5\cos^2\theta_\zeta)]\zeta^2 D_2(\zeta)\},
\end{aligned} \tag{50}
$$

$$
\frac{\omega}{u_\infty \cos\theta} = (\gamma_1 c_1 k_\infty - c_3)r^{-2}, \tag{51a}
$$

$$
\frac{u_r}{u_\infty \cos\theta} = 1 + c_1 r^{-1} + c_2 r^{-3}, \tag{51b}
$$

$$
\frac{u_\theta}{u_\infty \sin\theta} = -1 - \frac{1}{2}c_1 r^{-1} + \frac{1}{2}c_2 r^{-3}, \tag{51c}
$$

$$
\frac{\tau}{u_\infty \cos\theta} = c_3 r^{-2}, \tag{51d}
$$

where c_1, c_2, and c_3 are undetermined constants, and $A(\zeta)$, $B(\zeta)$, $D_1(\zeta)$, $D_2(\zeta)$, and $F(\zeta)$ are the solutions of the following integral equations, which are tabulated in Ref. 40 [$A(\zeta)$ and $B(\zeta)$ are first accurately obtained in Ref. 41] :

$$
\left.
\begin{aligned}
&\mathcal{L}[\zeta_i A(\zeta)] = -\zeta_i(\zeta^2 - \frac{5}{2}), \\
&\text{subsidiary condition:} \quad \int_0^\infty \zeta^4 A(\zeta)\exp(-\zeta^2)\,d\zeta = 0,
\end{aligned}
\right\} \tag{52}
$$

$$
\mathcal{L}[(\zeta_i\zeta_j - \frac{1}{3}\zeta^2\delta_{ij})B(\zeta)] = -2(\zeta_i\zeta_j - \frac{1}{3}\zeta^2\delta_{ij}), \tag{53}
$$

$$
\mathcal{L}[(\zeta_i\zeta_j - \frac{1}{3}\zeta^2\delta_{ij})F(\zeta)] = (\zeta_i\zeta_j - \frac{1}{3}\zeta^2\delta_{ij})A(\zeta), \tag{54}
$$

$$\mathcal{L}[(\zeta_i\delta_{jk} + \zeta_j\delta_{ki} + \zeta_k\delta_{ij})D_1(\zeta) + \zeta_i\zeta_j\zeta_k D_2(\zeta)]$$

$$= \gamma_1(\zeta_i\delta_{jk} + \zeta_j\delta_{ki} + \zeta_k\delta_{ij}) - \zeta_i\zeta_j\zeta_k B(\zeta), \tag{55}$$

$$\text{subsidiary condition} : \int_0^\infty [5\zeta^4 D_1(\zeta) + \zeta^6 D_2(\zeta)]\exp(-\zeta^2)d\zeta = 0.$$

The undetermined constants c_1, c_2, and c_3 are introduced since the information on the side of the sphere is not taken into account.

If r_D is taken larger than r_A, Eqs. (49) and (50) can be used to evaluate the boundary conditions (41) and (42). That is, by connecting $u_r/\cos\theta$, $u_\theta/\sin\theta$, and $\tau/\cos\theta$ in Eqs. (51b), (51c), and (51d) with $(u_r/\cos\theta)_{(I)}^{(n)}$, $(u_\theta/\sin\theta)_{(I)}^{(n)}$, and $(\tau/\cos\theta)_{(I)}^{(n)}$ obtained in the step (iv) of the process of solution in Sec. IV A respectively, we determine the constants c_1, c_2, and c_3 (say $c_1^{(n)}$, $c_2^{(n)}$, and $c_3^{(n)}$). Let Φ_c and $\widehat{\Phi}_s$ in Eqs. (49) and (50) with these constants be denoted by $\Phi_{cA}^{(n)}$ and $\widehat{\Phi}_{sA}^{(n)}$, respectively. We take $\Phi_{cA}^{(n)}$ (or $\widehat{\Phi}_{sA}^{(n)}$) at $(r^{(I-1)}, \zeta^{(j)}, \theta_\zeta^{(k)})$ and $(r^{(I)}, \zeta^{(j)}, \theta_\zeta^{(k)})$ as $G_{c(j,k)}^{(n+1)}$ (or $G_{s(j,k)}^{(n+1)}$) and $H_{c(j,k)}^{(n+1)}$ (or $H_{s(j,k)}^{(n+1)}$) in Eq. (41) [Eq. (42)] respectively. Thus, the boundary conditions (41) and (42) for the finite difference method are computed.

V. RESULT AND DISCUSSION

A. Macroscopic variables

The macroscopic variables ω, u_r, u_θ, and τ have simple dependence on θ: u_θ is proportional to $\sin\theta$ and the others are proportional to $\cos\theta$ [see Eqs. (19a)-(19e)]. The result of numerical computation $u_r/u_\infty \cos\theta$ vs r is shown in Fig. 3a and Table I, $u_\theta/u_\infty \sin\theta$ in Fig. 3b and Table II, $\omega/u_\infty \cos\theta$ in Fig. 3c and Table III, and $\tau/u_\infty \cos\theta$ in Fig. 3d and Table IV. In these figures and tables, the two limiting solutions for $k_\infty = 0$ and $k_\infty = \infty$ (see Sec. III) are also shown. For comparison, the corresponding results for the BKW equation are shown in Figs. 4a-4d.

The uniform flow is retarded by the sphere, whose effect is larger for smaller Knudsen numbers. One may think the effect of sphere extends further in the gas for larger Knudsen numbers since the molecules reflected on the sphere proceed in the gas with less collisions for larger Knudsen numbers, but it is not so in a steady flow. In the free molecular flow, only the molecules that hit the sphere get the information of the existence of the sphere. That is, only the part $O(1/r^2)$ of the molecules is affected by the sphere. When the Knudsen number is very small, on the other hand, the molecules reflected on the sphere soon collide with other molecules, give them the information of the sphere, return to the sphere, and reflected there again. The collided molecules soon collide with other molecules and so on. Successively the effect of the sphere propagates into the gas and finally to all the molecules. As the Knudsen number increases, the molecules travel longer distance before collision and some of the molecules that return to the sphere for smaller Knudsen numbers do not return to the sphere. Thus, the effect of the sphere is weaker for larger Knudsen numbers in the steady flow, although in a transient process disturbances may propagate faster for larger Knudsen numbers.

The temperature is not uniform, and the nonuniformity is larger for larger Knudsen numbers. This is a typical effect of gas rarefaction called thermal polarization.[13] Obviously in the continuum limit ($k_\infty = 0$), the temperature is uniform in a slow flow where a quantity of the second order of the Mach number can be neglected. For $k_\infty = 0.1$ (a small Knudsen number), the variation τ of the temperature for the BKW model is the opposite sign to that for the hard-sphere molecular gas, although both are very small (Figs. 3d and 4d). To understand the thermal polarization, let us examine the velocity distribution function at forward stagnation

point ($r = 1$, $\theta = \pi$ for $U_\infty > 0$) for the free molecular flow. The distribution of the molecules leaving the sphere is the half ($\zeta_1 < 0$) of a stationary Maxwellian with temperature T_∞, and that of the incoming molecules is the part ($\zeta_1 > 0$) of the Maxwellian with temperature T_∞ and velocity U_∞. Thus the width of the distribution at the stagnation point is wider by the order of $U_\infty (> 0)$ than that of the distribution with temperature T_∞, which means the temperature of the gas at the stagnation point is higher than T_∞ by the order of U_∞.

B. Drag on the sphere

The force acting on the sphere is obtained by integrating the momentum flux, which is equivalent to stress in the linearized problem, over any surface enclosing the sphere. Let F_i be the force on the sphere and U_i [instead of a special $(U_\infty, 0, 0)$] be the uniform flow. Then,

$$F_i = p_\infty L^2 (2RT_\infty)^{-1/2} U_i \, h_D(k_\infty), \tag{56}$$

where $h_D(k_\infty)$, a function of k_∞, is given in Fig. 5 and Table V. For the free molecular flow $(k_\infty = \infty)$[4],

$$h_D(\infty) = 2\sqrt{\pi}(\pi + 8)/3, \tag{57a}$$

and for small Knudsen numbers,

$$h_D(k_\infty) = 6\pi\gamma_1 k_\infty (1 + \kappa_0 k_\infty), \tag{57b}$$

which is calculated from the asymptotic solution in Sec. III (For the BKW equation, another higher order term in k_∞ is obtained[10]). In Fig. 5 various results by Millikan's experiment or other methods are also shown for comparison. The result for the BKW equation is our recent detailed computation by the method similar to the present analysis but the difference from the results in Refs. 8, 12, and 14 is small (See Table VI). The way of comparing the results of different molecular models is not unique. The relation between the viscosity μ and the mean free path ℓ_∞ is given by $\mu = (\sqrt{\pi}/2)\gamma_1 p_\infty (2RT_\infty)^{-1/2}\ell_\infty$. Since γ_1 depends on molecular models [Eq. (27)], the result of comparison of a quantity (e.g., h_D) differs whether μ or ℓ_∞ is taken as the common independent variable. When μ is taken as the common independent variable, k_∞ for a hard-sphere molecular gas is related to k_∞ for the BKW model as

$$k_\infty(\text{BKW}) = 1.270042 k_\infty \ (\text{hard sphere}). \tag{58}$$

In the comparison of the drag in Fig. 5, the conversion formula (58) for the BKW model and a similar one for Millikan's result are used.

Recently the drag for $k_\infty \gtrsim 1$ has been reported in Ref. 24. The results seem to lie nearly on the same curve as ours (slightly larger for $k_\infty \sim 1$ and smaller for $k_\infty \sim 10$ than ours) in Fig. 5. In Ref. 24 the interest was the global quantity, i.e., the drag, and the kernel of the collision integral is expanded and truncated at the fourth term. The result in Ref. 24 is a numerical solution of the model Boltzmann equation with the truncated collision kernel. In the numerical analysis the discontinuity of the velocity distribution function is not taken into account. Both save a large amount of computation. Thus, the purpose and approach in Ref. 24 are different from ours, where we tried to solve the original equation faithfully.

The drags for the BKW model computed by different methods are compared in Table VI. The difference is not large as a whole. The variational result, though a very simple test function was used, agrees very well with our result, where the discontinuity is taken into account. In the integral equation approach in Ref. 12, the difficulty of the discontinuity is bypassed[42], but the temperature field is assumed to be uniform, which means that larger errors are expected

for larger k_∞, since the variation of the temperature is larger for larger k_∞ (cf. Fig. 4d). The approach in Ref. 24 shows the same tendency (smaller for large k_∞ and larger for moderate k_∞) as that for a hard-sphere molecular gas with the kernel truncation.

C. Velocity distribution function

The velocity distribution functions $\Phi_c E/u_\infty$ and $\widehat{\Phi}_s E/u_\infty$ at several points in the gas are shown for $k_\infty = 0.1$, 1, and 10 in Figs. 6-11. The $\Phi_c E/u_\infty$ and $\widehat{\Phi}_s E/u_\infty$ of the uniform flow at infinity, common to all k_∞, are shown in Fig. 12 for reference. The difference due to the Knudsen number is clear. At $k_\infty = \infty$ (the free molecular flow; Sec. III), two classes of molecules are distinct. That is, at a point (r), the molecules with velocity $0 \leq \theta_\zeta < \pi - \mathrm{Arcsin}(1/r)$ come directly from infinity, whose distribution is given by the part $[0 \leq \theta_\zeta < \pi - \mathrm{Arcsin}(1/r)]$ of the uniform flow in Fig. 12; the molecules with the other velocities come directly from the sphere, whose distribution is given in Fig. 13 [Eqs. (23) and (24)]. At $k_\infty = 10$ (a large Knudsen number) in Figs. 10 and 11, this feature is well preserved and only local correction is seen. In contrast to the free molecular flow, however, the discontinuity of the velocity distribution function on the sphere decays in a long distance owing to molecular collisions. At $k_\infty = 0.1$ (Figs. 6 and 7) the behavior is quite different. The discontinuity of the velocity distribution function on the sphere decays in a short distance (Fig. 6a $\rightarrow$ 6b $\rightarrow$ 6c; Fig. 7a $\rightarrow$ 7b $\rightarrow$ 7c), and it transforms completely into a distribution similar to that of the uniform flow in a fairly short distance (Fig. 6a $\rightarrow$ 6d; Fig. 7a $\rightarrow$ 7c). Further away from the sphere the change in the distribution is mainly in size but not in shape (Fig. 6e $\rightarrow$ 12a; Fig. 7c $\rightarrow$ 7d $\rightarrow$ 12b). At $k_\infty = 1$ (an intermediate Knudsen number), the behavior of the distribution retains more of the feature of $k_\infty = 10$. For $k_\infty = 1$ and 10, the velocity distribution function is, more or less, of similar shape to that of the uniform flow in a region where its discontinuity is vanishingly small. This shows that the flow is nearly in equilibrium there. On the other hand, for $k_\infty = 0.1$, the decay of the discontinuity is so fast that the velocity distribution function undergoes thorough transformation in a region where the discontinuity is vanishingly small. This kinetic transition region is the Knudsen layer, and the region with discontinuity is the S layer at the bottom of the Knudsen layer, discussed in Refs. 26 and 27.

In order to show the decay of the discontinuity with distance clearly, $\Phi_c E/u_\infty$ and $\widehat{\Phi}_s E/u_\infty$ in $r\theta_\zeta$ plane at a given ζ are shown in Figs. 14-17. The Φ_c/u_∞ and $\widehat{\Phi}_s/u_\infty$ expressing the uniform flow at infinity are given by $\Phi_c/u_\infty = -2\zeta \cos\theta_\zeta$ and $\widehat{\Phi}_s/u_\infty = -2\zeta \sin\theta_\zeta$ [cf. Eq. (18)]. These sinusoidal surfaces are disturbed by the sphere, which imposes the condition (17). The discontinuity of ϕ decays monotonically with distance [cf. Eq. (20)]. This does not mean that the discontinuities of Φ_c and $\widehat{\Phi}_s (= \zeta \sin\theta_\zeta \Phi_s)$ decay monotonically because of the interaction terms between Φ_c and Φ_s in Eqs. (11) and (12). The discontinuity is smaller and decays in shorter distance for smaller Knudsen numbers (Figs. 14-16). Figures 15 and 17 show that the discontinuity decays more rapidly for smaller molecular speed. This reflects the fact that the discontinuity decays in the scale of the free path (but not the mean free path). At $k_\infty = 1$ and 10 (Figs. 15 and 16), the discontinuity extends to a point of the order of the mean free path from the sphere, but at $k_\infty = 0.1$ (Fig. 14), it extends only to a point much nearer than a point of the order of the mean free path from the sphere. This is because the discontinuity is nearly parallel near the sphere and decays in a distance of the order of the free path. This very thin layer with discontinuity for small Knudsen numbers corresponds to the S layer at the bottom of the Knudsen layer. The figures for the BKW model corresponding to Figs. 14-17 are given in Ref. 26. They are quite similar to the present results. For example, the figure for the BKW model corresponding to Fig. 15 is given in Fig. 18.

D. Lattice data and accuracy test

The data of the lattice system that was used to obtain the results in Secs. V A, B, and C are summarized. The typical examples of the size of physical space r_D and the lattice are shown in Table VII. The number of section is commonly 300 for all k_∞. The molecular speed is considered in $0 \leq \zeta \leq \zeta_D$ with $\zeta_D = 5$, and the interval is divided into 24 sections, i.e., $\zeta^{(i)} = \zeta_D(i/J)^2$ with $J = 24$. The region $0 \leq \theta_\zeta \leq \pi$ is divided into uniform 176 sections, i.e., $\widehat{K} = 88$ and $K = 176$. In this lattice the molecular velocity space $\zeta\theta_\zeta$ has 4425 lattice points, which means that 4425 terms are taken in the series (43) and (44).[43] The criterion of convergence of the sequences $\Phi_c^{(n)}$ and $\widehat{\Phi}_s^{(n)}$ is that the variations of the macroscopic variables $(\omega/u_\infty \cos\theta)^{(n)}$, $(u_r/u_\infty \cos\theta)^{(n)}$, $(u_\theta/u_\infty \sin\theta)^{(n)}$, and $(\tau/u_\infty \cos\theta)^{(n)}$ in 10 iterations are less than 5×10^{-7}.

It is inefficient, and also impossible in the present circumstances, to carry out extensive direct accuracy tests by various lattice systems on the basis of the Boltzmann equation for hard-sphere molecules since the computation is very large. The errors come from two different type of sources: computation of the collision integral and numerical integration of the differential system. For the latter the BKW equation is a guide. We therefore investigate the same problem by the same method on the basis of the BKW equation for various lattice systems, which can be carried out by engineering workstations such as MIPS RS 3230 and HP 9000 730. The typical data showing the dependence of the results on lattice systems are given in Table VIII, where the maximum differences of the macroscopic variables $\omega/u_\infty \cos\theta$, $u_r/u_\infty \cos\theta$, $u_\theta/u_\infty \sin\theta$, and $\tau/u_\infty \cos\theta$ by the use of different lattice systems over the whole flow field are shown. In the original computation of $\mathcal{L}_1$ and $\mathcal{L}_2$, the discontinuity of the velocity distribution function is not taken into account since the error of the integrand lies only between two lattice points $\theta_\zeta^{(2\kappa)} \leq \theta_\zeta < \theta_\zeta^{(2\kappa+2)}$ (cf. Sec. IV B). This error is tested for the BKW equation. The results are also shown in Table VIII. From the data in our previous works (Refs. 34, 37, etc.) on the Boltzmann equation for hard-sphere molecules, in addition to the above tests on BKW equation, we have chosen the lattice system mentioned in the first paragraph of this subsection.

Now return to solutions of the Boltzmann equation for hard-sphere molecules. The magnitude of $\Phi_c E/u_\infty$ and $\widehat{\Phi}_s E/u_\infty$ at $\zeta = 3.828$ is less than 6×10^{-7} for any r, θ_ζ, and k_∞, and therefore the size $\zeta_D(= 5)$ adopted in the present analysis is sufficiently large. Two tests for different lattice systems are carried out. In the test 1 (T1), the first 241 $r^{(i)}$ lattice points ($i = 0 - 240$) among 301 are reduced to 161, and in the test 2 (T2), the original 176 divisions of $0 \leq \theta_\zeta \leq \pi$ are reduced to 132 divisions. The results of both computations of the macroscopic variables $\omega/u_\infty \cos\theta$, $u_r/u_\infty \cos\theta$, $u_\theta/u_\infty \sin\theta$, and $\tau/u_\infty \cos\theta$ are compared with those on the original lattice system. Their maximum differences over the whole flow field are shown in Table IX, where the maximum values of the corresponding variables over the whole flow field are also given for reference. The lattice for θ_ζ seems to be sufficient. In the intermediate Knudsen numbers, more $r^{(i)}$ lattices are required to get the result of the same accuracy. This feature is consistent with that of the BKW equation.

The collision integral vanishes for Maxwellian distributions ($\phi = 1$, ζ_i, or ζ_j^2). For corresponding Φ_c and $\widehat{\Phi}_s$, therefore,

$$\left.\begin{array}{l} C_{(i,j,k)} = \nu_{(j)}\Phi_{c(i,j,k)}, \\[2ex] \widehat{S}_{(i,j,k)} = \nu_{(j)}\widehat{\Phi}_{s(i,j,k)}. \end{array}\right\} \tag{59}$$

The maximum differences between the computed and exact values of $(CE)_{(i,j,k)}$ and $(\widehat{S}E)_{(i,j,k)}$ for $\Phi_c = 1$, $\zeta\cos\theta_\zeta$, ζ^2, and $\widehat{\Phi}_s = \zeta\sin\theta_\zeta$ are 3.3×10^{-5}, 1.4×10^{-5}, 5.8×10^{-6}, and 5.2×10^{-5},

respectively. Incidentally, the maximums of $\nu(\zeta)E$, $\nu(\zeta)\zeta E\cos\theta_\zeta$, $\nu(\zeta)\zeta^2 E$, and $\nu(\zeta)\zeta E\sin\theta_\zeta$ are about 0.13, 0.06, 0.06, and 0.06 respectively.

The drag on the sphere can be computed by integrating the momentum flux over any surface enclosing the sphere. In principle this serves a good accuracy test of computation. In practice it is too severe in a three-dimensional problem in an infinite domain such as the present one to be applied to an arbitrarily large control surface. For a large control surface, the drag is obtained as a small quantity multiplied by a large area. Thus, the error in local variables is multiplied by the factor r_c^2, where r_c is the characteristic linear dimension of the control surface. The results in Table. V are computed on the sphere $r = 1$. In the tests for the control spheres $r = r^{(i)}$ for all $r^{(i)}$ between 1 and 4, the variation (max $-$ min) of h_D is less than 0.15% of h_D for $k_\infty = 0.2 - 10$ (0.56% for $k_\infty = 0.1$, 3.1% for $k_\infty = 0.05$). Another test to confirm the result of h_D was made for the BKW equation: The drag computed with the lattice system of double $r^{(i)}$ points (601) remains constant with width 0.26% allowance for the control surfaces $r = r^{(i)}$ with $r^{(i)} = 1 - 10$. The data for $r^{(i)} = 1 - 4$ are essentially the same as those computed with the original system of 301 $r^{(i)}$ lattice points.

A practical point that was introduced to improve the accuracy of numerical computation is added here. The solution approaches the uniform flow at infinity fairly slowly, and therefore for a wide range of r ($< r_D$), the difference between the solution and its asymptotic solution is fairly small. We consider the difference ϕ':

$$\left.\begin{array}{l} \phi' = \phi - \phi_a, \\[2mm] \phi_a/u_\infty = 2(1 + c_1 r^{-1})\zeta_1 + c_1 r^{-1}\zeta_\theta\sin\theta, \end{array}\right\} \tag{60}$$

where ϕ_a corresponds to the terms up to $O(1/r)$ in Eqs. (49) and (50). Then, from Eq. (1)

$$\zeta_i\frac{\partial\phi'}{\partial x_i} = \frac{1}{k_\infty}\mathcal{L}(\phi') - \zeta_i\frac{\partial\phi_a}{\partial x_i}, \tag{61}$$

where $\mathcal{L}(\phi_a)$ term disappears since ϕ_a is a local Maxwellian. Over a wide range, $|\phi'|$ is fairly smaller than $|\phi|$, and correspondingly the error of $\mathcal{L}(\phi')$ is fairly smaller than that of $\mathcal{L}(\phi)$. Furthermore, by analyzing Eq. (61) instead of Eq. (1), we can avoid the error accumulated by long range integration to form the slowly varying dominant part ϕ_a for large r (cf. footnote 39 in Ref. 25).

The computation was carried out by HP 9000 730 and MIPS RS 3230 at our laboratory (for the BKW equation) and FACOM VP-2600 computer at the Data Processing Center of Kyoto University (for the Boltzmann equation for hard-sphere molecules).

VI. CONCLUDING REMARKS

We have investigated the behavior of a rarefied gas around a spherical body set in a uniform flow on the basis of the linearized Boltzmann equation for hard-sphere molecules and the diffuse reflection boundary condition. With the aid of the similarity solution, the original linearized Boltzmann equation with six independent variables is reduced to two simultaneous integro-differential equations with three independent variables. These equations are solved numerically by a finite-difference method. The computation of the collision integral, which takes the majority of the computing time, is carried out efficiently by the numerical kernel method. The data of the kernel stored can be applied to other computations. Thus, we have obtained the comprehensive and accurate information of the flow field, including the velocity distribution function with

discontinuity, and the force acting on the sphere for the whole range of the Knudsen number. The S layer at the bottom of the Knudsen layer is discussed by the behavior of the velocity distribution function.

The velocity distribution function of the gas molecules has a discontinuity in the gas, which is of considerable size and extends to a wide region for intermediate and large Knudsen numbers. This is a typical feature of a gas around a convex body. Thus it introduces another difficulty in analysis of rarefied gas flow problems. Some of the results of the present analysis are compared with those of the BKW model equation. In view of the result of comparison and the simplicity of the BKW equation, for which the analysis of the present problem can be carried out by engineering workstations such as MIPS RS 3230, it is a nice equation to be used in engineering problems.

In the present analysis, the temperature of the sphere is assumed to be equal to that of the gas at infinity. This is realized without any special device when the thermal conductivity of the sphere is much larger than that of the gas. In this case the temperature of the sphere is uniform and the energy flow from the sphere vanishes since the sphere cannot be a source or sink of energy in a steady state. From the similarity solution, the latter condition is seen to be satisfied by the present solution, where the temperature of the sphere is the same as that of the gas at infinity. When the sphere is kept at a different temperature, a spherically symmetric solution should be superimposed. This does not influence the velocity field and the drag on the sphere.

REFERENCES

1. R. A. Millikan, "The isolation of an ion, a precision measurement of its charge, and the correction of Stokes's law," Phys. Rev. **32**, 349 (1911).
2. M. Knudsen and S. Weber, "Luftwiderstand gegen die langsame Bewegung kleiner Kugeln," Ann. der Phys. **36**, 981 (1911).
3. R. A. Millikan, "The general law of fall of a small spherical body through a gas, and its bearing upon the nature of molecular reflection from surfaces," Phys. Rev. 2nd Ser. **22**, 1 (1923).
4. P. S. Epstein, "On the resistance experienced by spheres in their motion through gases," Phys. Rev. 2nd Ser. **23**, 710 (1924).
5. R. Goldberg, "The flow of a rarefied perfect gas past a fixed spherical obstacle," Ph. D. Thesis, New York Univ. (1954).
6. A. B. Basset, *Hydrodynamics* (Dover, New York, 1961), Vol. II, p. 271.
7. D. R. Willis, "Sphere drag at high Knudsen number and low Mach number," Phys. Fluids **9**, 2522 (1966).
8. C. Cercignani, C. D. Pagani, and P. Bassanini, "Flow of a rarefied gas past an axisymmetric body. II. Case of a sphere," Phys. Fluids **11**, 1399 (1968).
9. W. Phillips, "Drag force on a small sphere moving through a gas," Phys. Fluids **18**, 1089 (1975).
10. Y. Sone and K. Aoki, "Forces on a spherical particle in a slightly rarefied gas," in *Rarefied Gas Dynamics*, edited by J. L. Potter (AIAA, New York, 1977), Part 1, p. 417.
11. Y. Sone and K. Aoki, "Slightly rarefied gas flow over a specularly reflecting body," Phys. Fluids **20**, 571 (1977).
12. K. C. Lea and S. K. Loyalka, "Motion of a sphere in a rarefied gas," Phys. Fluids **25**, 1550 (1982).
13. S. P. Bakanov, V. V. Vysotskij, B. J. Derjaguin, and V. I. Roldughin, "Thermal polarization of bodies in the rarefied gas flow," J. Non-Equilib. Thermodyn. **8**, 75 (1983).

14. W. S. Law and S. K. Loyalka, "Motion of a sphere in a rarefied gas. II. Role of temperature variation in the Knudsen layer," Phys. Fluids **29**, 3886 (1986).

15. K. Aoki and Y. Sone, "Temperature field induced around a sphere in a uniform flow of a rarefied gas," Phys. Fluids **30**, 2286 (1987).

16. S. A. Beresnev, V. G. Chernyak, and G. A. Fomyagin, "Motion of a spherical particle in a rarefied gas. Part 2. Drag and thermal polarization," J. Fluid Mech. **219**, 405 (1990).

17. C. Cercignani and C. D. Pagani, "Flow of a rarefied gas past an axisymmetric body. I. General remarks," Phys. Fluids **11**, 1395 (1968).

18. P. L. Bhatnagar, E. P. Gross, and M. Krook, "A model for collision processes in gases, I," Phys. Rev. **94**, 511 (1954).

19. P. Welander, "On the temperature jump in a rarefied gas," Ark. Fys. **7**, 507 (1954).

20. In this paragraph, we consider the case where the temperature of the sphere is the same as that of the uniform flow (or the particle has very high thermal conductivity) and the speed of uniform flow is so low that the quantities of the order of the Mach number squared are negligible.

21. Y. Sone, "Asymptotic theory of flow of rarefied gas over a smooth boundary I," in *Rarefied Gas Dynamics*, edited by L. Trilling and H. Y. Wachman (Academic, New York, 1969), Vol. 1, p. 243.

22. Y. Sone, "Asymptotic theory of flow of rarefied gas over a smooth boundary II," in *Rarefied Gas Dynamics*, edited by D. Dini (Editrice Tecnico Scientifica, Pisa, 1971), Vol. 2, p. 737.

23. S. Takata, Y. Sone, and K. Aoki, "Drag and thermal force on a spherical particle in a rarefied gas – Numerical analysis for all Knudsen numbers –," J. Vac. Soc. Jpn. **35**, 143 (1992) (in Japanese).

24. S. K. Loyalka, "Motion of a sphere in a gas: Numerical solution of the linearized Boltzmann equation," Phys. Fluids A **4**, 1049 (1992).

25. H. Sugimoto and Y. Sone, "Numerical analysis of steady flows of a gas evaporating from its cylindrical condensed phase on the basis of kinetic theory," Phys. Fluids A **4**, 419 (1992).

26. Y. Sone and S. Takata, "Discontinuity of the velocity distribution function in a rarefied gas around a convex body and the S layer at the bottom of the Knudsen layer," Transp. Theory Stat. Phys. **21**, 501 (1992).

27. Y. Sone, "New kind of boundary layer over a convex solid boundary in a rarefied gas," Phys. Fluids **16**, 1422 (1973).

28. H. Grad, "Asymptotic theory of the Boltzmann equation, II," in *Rarefied Gas Dynamics*, edited by J. A. Laurmann (Academic, New York, 1963), Vol. 1, p. 26.

29. C. Cercignani, *The Boltzmann Equation and Its Applications* (Springer, Berlin, 1987), Chap. IV, Sec. 5.

30. Y. Sone and K. Aoki, "Similarity solution of the linearized Boltzmann equation with application to thermophoresis of a spherical particle," J. Mec. Theor. Appl. **2**, 3 (1983).

31. Y. Sone, "Lecture Notes on Molecular Gas Dynamics," (Department of Aeronautical Engineering, Kyoto University, Kyoto, 1990) Chap. III (in Japanese).

32. Y. Sone and K. Aoki, "Steady gas flows past bodies at small knudsen numbers –Boltzmann and hydrodynamic systems–," Transp. Theory Stat. Phys. **16**, 189 (1987); "Asymptotic theory of slightly rarefied gas flow and force on a closed body," Mem. Fac. Eng. Kyoto Univ. **49**, 237 (1987).

33. Y. Sone, "Asymptotic theory of a steady flow of a rarefied gas past bodies for small knudsen numbers," in *Advances in Kinetic Theory and Continuum Mechanics*, edited by R. Gatignol and Soubbaramayer (Springer, Berlin, 1991), p. 19.

34. T. Ohwada, Y. Sone, and K. Aoki, "Numerical analysis of the shear and thermal creep flows of a rarefied gas over a plane wall on the basis of the linearized Boltzmann equation for

hard-sphere molecules," Phys. Fluids A **1**, 1588 (1989).

35. Y. Sone and Y. Onishi, "Kinetic theory of evaporation and condensation – Hydrodynamic equation and slip boundary condition –," J. Phys. Soc. Jpn. **44**, 1981 (1978).

36. This means that $\Phi^{(n)}_{c(0,j,\widehat{K})}$ and $\widehat{\Phi}^{(n)}_{s(0,j,\widehat{K})}$ should be taken as the limiting values for $\theta_\zeta \to \pi/2-0$. The other limiting values are given by Eq. (17)

37. Y. Sone, T. Ohwada, and K. Aoki, "Temperature jump and Knudsen layer in a rarefied gas over a plane wall: Numerical analysis of the linearized Boltzmann equation for hard-sphere molecules," Phys. Fluids A **1**, 363 (1989).

38. $\Psi_{\ell m}(\zeta, \theta_\zeta)$ corresponds to $\Psi_{\ell m}(\zeta_1, \zeta_r)$ in Ref. 37 with replacement $(\zeta \to \zeta_1,\ \theta_\zeta \to \zeta_r)$.

39. The integration with respect to $\bar\psi$ in $\mathcal{L}^c_2$ and $\mathcal{L}^s_2$ can be carried out analytically. After a similar transformation in Ref. 34 and detailed classification of the cases depending on the relative position of the singularity to the ring, the integrations are carried out by Gauss-Legendre formula.

40. T. Ohwada and Y. Sone, "Analysis of thermal stress slip flow and negative thermophoresis using the Boltzmann equation for hard-sphere molecules," Eur. J. Mech., B/Fluids, **11**, 389 (1992).

41. C. L. Pekeris and Z. Alterman, "Solution of the Boltzmann-Hilbert integral equation II. the coefficients of viscosity and heat conduction," Proc. Natl. Acad. Sci. **43**, 998 (1957).

42. For the BKW equation with the diffuse reflection condition, the velocity distribution function can be eliminated, and the integral equations for ω, u_i, and τ, which are continuous, are derived. They are analyzed in Ref. 12.

43. The operators $\mathcal{L}^c_1$, $\mathcal{L}^c_2$, $\mathcal{L}^s_1$, and $\mathcal{L}^s_2$ in Eqs. (14a)-(15b) have a symmetric property: $\mathcal{L}^c_1[\Phi(r,\xi,\theta_\xi)]_{(r,\zeta,\theta_\zeta)} = \mathcal{L}^c_1[\Phi(r,\xi,(\pi-\theta_\xi))]_{(r,\zeta,\pi-\theta_\zeta)}$ etc. For a uniform θ_ζ lattice system, therefore, $K^c_{jk\ell m} = K^c_{j(K-k)\ell(K-m)}$, and $K^s_{jk\ell m} = K^s_{j(K-k)\ell(K-m)}$. Thus only $K^c_{jk\ell m}$ and $K^s_{jk\ell m}$ $(0 \le m \le \widehat{K},\ 0 \le k \le K,\ 0 \le j,\ \ell \le J)$, 9,845,625 each, need to be prepared.

TABLE I. The distribution of the radial flow velocity $(u_r/u_\infty \cos\theta$ vs $r)$ for various k_∞. The data are interpolated with sufficient accuracy from those at the lattice points, which are not common for different k_∞.

r \ k_∞	$u_r/u_\infty \cos\theta$											
	0	0.05	0.1	0.2	0.4	0.6	1	2	4	6	10	∞
1	0.0000	0.0000	0.0000	0.0000	0.0000	0.0000	0.0000	0.0000	0.0000	0.0000	0.0000	0.0000
1.01	0.0001	0.0015	0.0025	0.0040	0.0060	0.0072	0.0086	0.0099	0.0106	0.0109	0.0111	0.0113
1.1	0.0120	0.0245	0.0347	0.0500	0.0702	0.0831	0.0973	0.1113	0.1190	0.1215	0.1236	0.1263
1.2	0.0394	0.0600	0.0779	0.1050	0.1417	0.1651	0.1914	0.2170	0.2314	0.2360	0.2398	0.2448
1.3	0.0737	0.0994	0.1224	0.1578	0.2065	0.2380	0.2734	0.3080	0.3273	0.3335	0.3386	0.3453
1.4	0.1108	0.1393	0.1658	0.2068	0.2640	0.3014	0.3435	0.3848	0.4078	0.4152	0.4212	0.4291
1.5	0.1481	0.1782	0.2068	0.2515	0.3146	0.3562	0.4034	0.4495	0.4751	0.4835	0.4902	0.4990
1.7	0.2194	0.2502	0.2808	0.3290	0.3988	0.4454	0.4985	0.5507	0.5797	0.5893	0.5967	0.6066
2	0.3125	0.3420	0.3725	0.4211	0.4932	0.5424	0.5988	0.6547	0.6858	0.6961	0.7039	0.7145
2.5	0.4320	0.4577	0.4856	0.5304	0.5987	0.6466	0.7021	0.7578	0.7888	0.7992	0.8070	0.8174
3	0.5185	0.5407	0.5656	0.6056	0.6678	0.7122	0.7641	0.8169	0.8464	0.8564	0.8638	0.8736
4	0.6328	0.6498	0.6696	0.7016	0.7525	0.7898	0.8339	0.8796	0.9057	0.9144	0.9210	0.9294
5	0.7040	0.7177	0.7337	0.7601	0.8025	0.8342	0.8717	0.9113	0.9343	0.9420	0.9478	0.9551
7	0.7872	0.7971	0.8083	0.8276	0.8591	0.8831	0.9115	0.9423	0.9606	0.9668	0.9715	0.9773
10	0.8505	0.8575	0.8651	0.8785	0.9012	0.9187	0.9393	0.9621	0.9761	0.9809	0.9845	0.9889
15	0.9001	0.9048	0.9096	0.9185	0.9338	0.9458	0.9600	0.9757	0.9857	0.9892	0.9919	0.9951
20	0.9251	0.9286	0.9321	0.9386	0.9501	0.9593	0.9700	0.9821	0.9898	0.9925	0.9946	0.9973
25	0.9400	0.9428	0.9456	0.9508	0.9599	0.9673	0.9760	0.9857	0.9920	0.9943	0.9961	0.9983
50	0.9700	0.9714	0.9728	0.9753	0.9796	0.9833	0.9878	0.9929	0.9961	0.9974	0.9983	0.9996
100	0.9850	0.9857	0.9864	0.9876	0.9897	0.9915	0.9937	0.9963	0.9981	0.9987	0.9992	0.9999
200	0.9925	0.9929	0.9932	0.9938	0.9948	0.9957	0.9968	0.9981	0.9990	0.9993	0.9996	1.0000
500	0.9970	0.9971	0.9973	0.9975	0.9979	0.9983	0.9987	0.9992	0.9996	0.9997	0.9999	1.0000

TABLE II. The distribution of the θ component of the flow velocity $(u_\theta/u_\infty \sin\theta$ vs $r)$ for various k_∞. The data are interpolated with sufficient accuracy from those at the lattice points, which are not common for different k_∞.

r \ k_∞	$u_\theta/u_\infty \sin\theta$											
	0	0.05	0.1	0.2	0.4	0.6	1	2	4	6	10	∞
1	0.0000	−0.0598	−0.1078	−0.1777	−0.2662	−0.3206	−0.3805	−0.4379	−0.4696	−0.4801	−0.4884	−0.5000
1.01	−0.0148	−0.0854	−0.1403	−0.2216	−0.3272	−0.3929	−0.4658	−0.5362	−0.5751	−0.5882	−0.5984	−0.6128
1.1	−0.1304	−0.1996	−0.2598	−0.3512	−0.4748	−0.5539	−0.6425	−0.7285	−0.7763	−0.7922	−0.8047	−0.8219
1.2	−0.2303	−0.2890	−0.3448	−0.4317	−0.5531	−0.6322	−0.7215	−0.8084	−0.8566	−0.8725	−0.8850	−0.9021
1.3	−0.3093	−0.3592	−0.4095	−0.4895	−0.6042	−0.6804	−0.7668	−0.8512	−0.8979	−0.9133	−0.9253	−0.9417
1.4	−0.3732	−0.4163	−0.4616	−0.5345	−0.6418	−0.7141	−0.7965	−0.8774	−0.9222	−0.9370	−0.9484	−0.9639
1.5	−0.4259	−0.4636	−0.5047	−0.5712	−0.6710	−0.7393	−0.8177	−0.8948	−0.9376	−0.9517	−0.9625	−0.9772
1.7	−0.5079	−0.5378	−0.5721	−0.6280	−0.7146	−0.7755	−0.8460	−0.9161	−0.9551	−0.9679	−0.9777	−0.9908
2	−0.5938	−0.6163	−0.6437	−0.6883	−0.7595	−0.8111	−0.8717	−0.9330	−0.9672	−0.9784	−0.9870	−0.9983
2.5	−0.6840	−0.6999	−0.7203	−0.7534	−0.8075	−0.8482	−0.8967	−0.9470	−0.9756	−0.9849	−0.9920	−1.0011
3	−0.7407	−0.7531	−0.7692	−0.7954	−0.8389	−0.8723	−0.9124	−0.9549	−0.9795	−0.9876	−0.9936	−1.0014
4	−0.8086	−0.8174	−0.8284	−0.8470	−0.8782	−0.9027	−0.9321	−0.9645	−0.9837	−0.9902	−0.9949	−1.0009
5	−0.8480	−0.8550	−0.8631	−0.8775	−0.9020	−0.9213	−0.9444	−0.9704	−0.9863	−0.9916	−0.9956	−1.0006
7	−0.8921	−0.8972	−0.9023	−0.9122	−0.9294	−0.9431	−0.9592	−0.9776	−0.9894	−0.9935	−0.9965	−1.0003
10	−0.9248	−0.9283	−0.9315	−0.9382	−0.9501	−0.9597	−0.9708	−0.9836	−0.9920	−0.9950	−0.9973	−1.0001
15	−0.9499	−0.9523	−0.9544	−0.9586	−0.9664	−0.9728	−0.9802	−0.9887	−0.9943	−0.9964	−0.9980	−1.0000
20	−0.9625	−0.9642	−0.9659	−0.9690	−0.9745	−0.9794	−0.9850	−0.9913	−0.9956	−0.9972	−0.9984	−1.0000
25	−0.9700	−0.9714	−0.9727	−0.9752	−0.9794	−0.9833	−0.9879	−0.9930	−0.9964	−0.9977	−0.9987	−1.0000
50	−0.9850	−0.9857	−0.9864	−0.9876	−0.9895	−0.9914	−0.9937	−0.9964	−0.9981	−0.9988	−0.9993	−1.0000
100	−0.9925	−0.9929	−0.9932	−0.9938	−0.9948	−0.9956	−0.9967	−0.9981	−0.9990	−0.9994	−0.9996	−1.0000
200	−0.9962	−0.9964	−0.9966	−0.9969	−0.9974	−0.9978	−0.9983	−0.9990	−0.9995	−0.9997	−0.9998	−1.0000
500	−0.9985	−0.9986	−0.9986	−0.9988	−0.9990	−0.9991	−0.9993	−0.9996	−0.9998	−0.9999	−0.9999	−1.0000

TABLE III. The distribution of the density $(\omega/u_\infty \cos\theta$ vs $r)$ for various k_∞. The data are interpolated with sufficient accuracy from those at the lattice points, which are not common for different k_∞.

	$\omega/u_\infty \cos\theta$										
$r \diagdown k_\infty$	0.05	0.1	0.2	0.4	0.6	1	2	4	6	10	∞
1	−0.0925	−0.1842	−0.3522	−0.6128	−0.7897	−0.9968	−1.2055	−1.3263	−1.3683	−1.4016	−1.4504
1.01	−0.0886	−0.1740	−0.3272	−0.5622	−0.7214	−0.9076	−1.0949	−1.2034	−1.2410	−1.2708	−1.3967
1.1	−0.0730	−0.1396	−0.2543	−0.4266	−0.5432	−0.6797	−0.8170	−0.8964	−0.9239	−0.9457	−1.2014
1.2	−0.0613	−0.1158	−0.2076	−0.3435	−0.4354	−0.5429	−0.6513	−0.7137	−0.7356	−0.7526	−1.0501
1.3	−0.0523	−0.0982	−0.1743	−0.2855	−0.3605	−0.4484	−0.5371	−0.5881	−0.6061	−0.6200	−0.9311
1.4	−0.0451	−0.0845	−0.1490	−0.2421	−0.3048	−0.3784	−0.4523	−0.4951	−0.5101	−0.5218	−0.8345
1.5	−0.0394	−0.0735	−0.1291	−0.2085	−0.2617	−0.3240	−0.3872	−0.4235	−0.4363	−0.4461	−0.7545
1.7	−0.0308	−0.0572	−0.0999	−0.1598	−0.1997	−0.2464	−0.2938	−0.3210	−0.3306	−0.3380	−0.6301
2	−0.0223	−0.0413	−0.0719	−0.1139	−0.1417	−0.1741	−0.2069	−0.2259	−0.2324	−0.2377	−0.5011
2.5	−0.0143	−0.0264	−0.0459	−0.0722	−0.0894	−0.1091	−0.1291	−0.1409	−0.1447	−0.1479	−0.3691
3	−0.0100	−0.0183	−0.0318	−0.0499	−0.0616	−0.0749	−0.0883	−0.0964	−0.0988	−0.1010	−0.2897
4	−0.0056	−0.0103	−0.0178	−0.0279	−0.0344	−0.0417	−0.0489	−0.0531	−0.0545	−0.0556	−0.2003
5	−0.0036	−0.0066	−0.0114	−0.0178	−0.0219	−0.0266	−0.0311	−0.0337	−0.0345	−0.0351	−0.1520
7	−0.0019	−0.0033	−0.0058	−0.0091	−0.0111	−0.0135	−0.0158	−0.0170	−0.0174	−0.0177	−0.1017
10	−0.0009	−0.0016	−0.0028	−0.0044	−0.0054	−0.0066	−0.0077	−0.0083	−0.0085	−0.0086	−0.0676
15	−0.0004	−0.0007	−0.0012	−0.0019	−0.0024	−0.0029	−0.0034	−0.0037	−0.0037	−0.0038	−0.0432
20	−0.0002	−0.0004	−0.0007	−0.0011	−0.0013	−0.0016	−0.0019	−0.0021	−0.0021	−0.0022	−0.0317
25	−0.0001	−0.0003	−0.0004	−0.0007	−0.0008	−0.0010	−0.0012	−0.0013	−0.0013	−0.0014	−0.0250
50	−0.0000	−0.0001	−0.0001	−0.0002	−0.0002	−0.0002	−0.0003	−0.0003	−0.0003	−0.0003	−0.0122
100		−0.0000	−0.0000	−0.0000	−0.0000	−0.0001	−0.0001	−0.0001	−0.0001	−0.0001	−0.0060
200						−0.0000	−0.0000	−0.0000	−0.0000	−0.0000	−0.0030
500								−0.0000	−0.0000	−0.0000	−0.0012

TABLE IV. The distribution of the temperature $(\tau/u_\infty \cos\theta$ vs $r)$ for various k_∞. The data are interpolated with sufficient accuracy from those at the lattice points, which are not common for different k_∞.

	$\tau/u_\infty \cos\theta$										
$r \diagdown k_\infty$	0.05	0.1	0.2	0.4	0.6	1	2	4	6	10	∞
1	−0.0010	−0.0058	−0.0236	−0.0620	−0.0903	−0.1233	−0.1551	−0.1724	−0.1780	−0.1822	−0.1881
1.01	−0.0006	−0.0045	−0.0203	−0.0567	−0.0843	−0.1172	−0.1496	−0.1675	−0.1734	−0.1780	−0.1844
1.1	−0.0002	−0.0029	−0.0148	−0.0440	−0.0670	−0.0951	−0.1235	−0.1396	−0.1450	−0.1493	−0.1554
1.2	−0.0002	−0.0023	−0.0118	−0.0358	−0.0550	−0.0786	−0.1028	−0.1167	−0.1214	−0.1252	−0.1306
1.3	−0.0001	−0.0019	−0.0098	−0.0299	−0.0462	−0.0663	−0.0870	−0.0990	−0.1032	−0.1065	−0.1128
1.4	−0.0001	−0.0016	−0.0084	−0.0255	−0.0394	−0.0567	−0.0746	−0.0851	−0.0888	−0.0917	−0.0960
1.5	−0.0001	−0.0014	−0.0072	−0.0220	−0.0340	−0.0490	−0.0647	−0.0739	−0.0772	−0.0797	−0.0836
1.7	−0.0000	−0.0011	−0.0056	−0.0169	−0.0262	−0.0378	−0.0500	−0.0573	−0.0599	−0.0619	−0.0651
2	−0.0000	−0.0008	−0.0041	−0.0121	−0.0187	−0.0270	−0.0358	−0.0412	−0.0431	−0.0446	−0.0470
2.5	−0.0000	−0.0006	−0.0026	−0.0077	−0.0118	−0.0170	−0.0226	−0.0261	−0.0274	−0.0284	−0.0301
3	−0.0001	−0.0004	−0.0019	−0.0053	−0.0082	−0.0117	−0.0156	−0.0180	−0.0189	−0.0197	−0.0209
4	−0.0001	−0.0003	−0.0011	−0.0030	−0.0046	−0.0065	−0.0086	−0.0100	−0.0105	−0.0110	−0.0118
5	−0.0001	−0.0002	−0.0007	−0.0020	−0.0030	−0.0042	−0.0055	−0.0064	−0.0067	−0.0070	−0.0075
7	−0.0001	−0.0001	−0.0004	−0.0010	−0.0016	−0.0021	−0.0027	−0.0032	−0.0034	−0.0035	−0.0038
10		−0.0001	−0.0002	−0.0005	−0.0008	−0.0011	−0.0013	−0.0015	−0.0016	−0.0017	−0.0019
15			−0.0001	−0.0002	−0.0004	−0.0005	−0.0006	−0.0007	−0.0007	−0.0007	−0.0008
20			−0.0001	−0.0001	−0.0002	−0.0003	−0.0003	−0.0004	−0.0004	−0.0004	−0.0005
25			−0.0000	−0.0001	−0.0001	−0.0002	−0.0002	−0.0002	−0.0003	−0.0003	−0.0003
50				−0.0000	−0.0000	−0.0000	−0.0001	−0.0001	−0.0001	−0.0001	−0.0001
100					−0.0000	−0.0000	−0.0000	−0.0000	−0.0000	−0.0000	−0.0000
200							−0.0000	−0.0000	−0.0000	−0.0000	−0.0000
500								−0.0000	−0.0000	−0.0000	−0.0000

TABLE V. The drag on the sphere: h_D vs k_∞ [cf. Eq. (56)].

k_∞	0.05	0.1	0.2	0.4	0.6	1	2	4	6	10	∞
$h_D(k_\infty)$	1.1091	2.1168	3.8110	6.2292	7.7951	9.5625	11.2772	12.2333	12.5557	12.8071	13.1653

TABLE VI. Comparison of h_D in the drag formula (56) for the BKW model. The conversion (58) of k_∞ is not made here.

	$h_D(k_\infty)/h_D(\infty)$			
k_∞	Ref. 8	Ref. 12	Ref. 24	Present method
1	0.6404	0.6402	0.6476	0.6403
2	0.7900	0.7899	0.7933	0.7907
4	0.8864	0.8870	0.8859	0.8879
10	0.9529	0.9476	0.9508	0.9540

TABLE VII. Examples of lattice of r.

	$k_\infty = 0.1$			$k_\infty = 1$			$k_\infty = 10$	
i	$r^{(i)}$	$\Delta r^{(i)}$	i	$r^{(i)}$	$\Delta r^{(i)}$	i	$r^{(i)}$	$\Delta r^{(i)}$
1	1.000006	6.35×10^{-6}	1	1.000002	2.31×10^{-6}	1	1.000005	5.47×10^{-6}
20	1.0032	3.95×10^{-4}	20	1.0040	5.47×10^{-4}	20	1.0151	2.11×10^{-3}
54	1.05	2.74×10^{-3}	102	1.51	1.49×10^{-2}	145	6.02	1.02×10^{-1}
68	1.10	4.24×10^{-3}	128	2.01	2.35×10^{-2}	183	11.04	1.63×10^{-1}
87	1.21	7.00×10^{-3}	161	3.02	3.75×10^{-2}	218	20.86	8.75×10^{-1}
118	1.51	1.27×10^{-2}	200	6.10	2.27×10^{-1}	234	52.12	3.12
148	2.00	2.00×10^{-2}	214	11.20	4.99×10^{-1}	245	99.94	5.47
300	$13.77 (= r_D)$	2.70×10^{-1}	273	100.72	2.81	300	$928.72 (= r_D)$	27.00
			300	$199.26 (= r_D)$	4.49			

TABLE VIII. Dependence of the macroscopic variables on the lattice systems for the BKW model.

		Difference between the systems A and B[a]		
A	B	$k_\infty = 0.1$	$k_\infty = 1$	$k_\infty = 10$
$(Z1,R1,\bigcirc)$[b]	$(Z1,R3,\bigcirc)$	1×10^{-6}	2×10^{-6}	3×10^{-6}
$(Z1,R1,\bigcirc)$	$(Z1,R2,\bigcirc)$	3×10^{-4}	1×10^{-3}	6×10^{-4}
$(Z1,R1,\bigcirc)$	$(Z2,R1,\bigcirc)$	2×10^{-4}	3×10^{-4}	4×10^{-4}
$(Z2,R1,\bigcirc)$	$(Z2,R1,\times)$	3×10^{-5}	2×10^{-4}	2×10^{-4}

[a] Upper bounds of the differences of $\omega/u_\infty \cos\theta$, $u_r/u_\infty \cos\theta$, $u_\theta/u_\infty \sin\theta$, and $\tau/u_\infty \cos\theta$ for the systems A and B over the whole lattice points.

[b] Z1: $\zeta_D = 6$, $J = 24$, $K = 300$
Z2: $\zeta_D = 5$, $J = 24$, $K = 176$
R1: $I = 300$, $r_D = 13.77$ ($k_\infty = 0.1$), 199.26 ($k_\infty = 1$), 928.72 ($k_\infty = 10$)
R2: $I = 600$, $r_D = 13.77$ ($k_\infty = 0.1$), 199.26 ($k_\infty = 1$), 928.72 ($k_\infty = 10$)
R3: $I = 320$, $r_D = 20.38$ ($k_\infty = 0.1$), 304.52 ($k_\infty = 1$), 1589.87 ($k_\infty = 10$)
$\bigcirc$: In the computation of the macroscopic variables in the gain term of collision, the discontinuity of ϕ is taken into account.
$\times$: not taken into account.

TABLE IX. Dependence of the macroscopic variables on the lattice systems for the hard-sphere gas.

		$u_r/u_\infty \cos\theta$	$u_\theta/u_\infty \sin\theta$	$\omega/u_\infty \cos\theta$	$\tau/u_\infty \cos\theta$
$k_\infty = 0.1$	(T1)[a]	9.8×10^{-5}	1.9×10^{-4}	1.1×10^{-4}	1.7×10^{-5}
	(T2)[b]	9.5×10^{-5}	1.4×10^{-4}	8.8×10^{-5}	2.1×10^{-5}
	Maximum[c]	1	1	0.1842	0.0058
$k_\infty = 1$	(T1)	1.2×10^{-3}	1.3×10^{-3}	1.6×10^{-3}	2.2×10^{-4}
	(T2)	1.6×10^{-4}	1.3×10^{-4}	2.5×10^{-4}	6.6×10^{-5}
	Maximum	1	1	0.9968	0.1233
$k_\infty = 10$	(T1)	4.7×10^{-4}	3.4×10^{-4}	6.2×10^{-4}	4.0×10^{-5}
	(T2)	1.7×10^{-4}	1.5×10^{-4}	2.2×10^{-4}	1.8×10^{-5}
	Maximum	1	1	1.4016	0.1822

[a] Upper bounds of the differences of a macroscopic variable for the original lattice system (cf. first paragraph of Sec. V D) and for the system with reduced $r^{(i)}$ lattice points (cf. third paragraph of Sec. V D) over the whole lattice points.

[b] Upper bounds of the differences of a macroscopic variable for the original lattice system and for the system with reduced $\theta_\zeta^{(k)}$ lattice points (cf. third paragraph of Sec. V D) over the whole lattice points.

[c] Maximum of the absolute value.
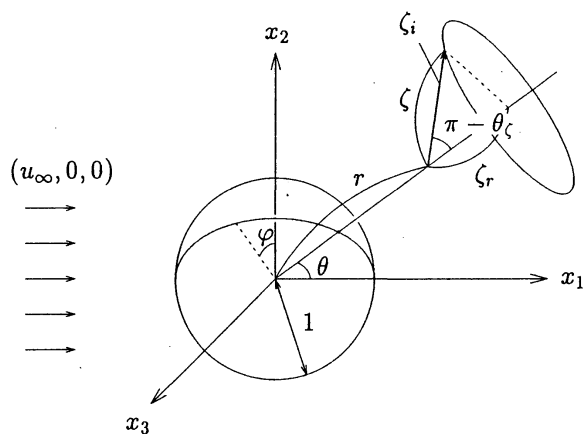
FIG. 1. Geometry and coordinate systems [Sec. II A and Eq. (8)].
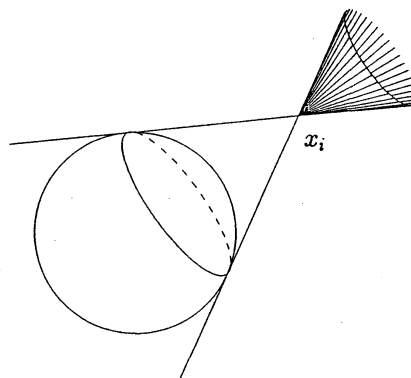
FIG. 2. Discontinuity of the velocity distribution function. At the point x_i, the velocity distribution function is discontinuous on the shaded cone in ζ_i space.
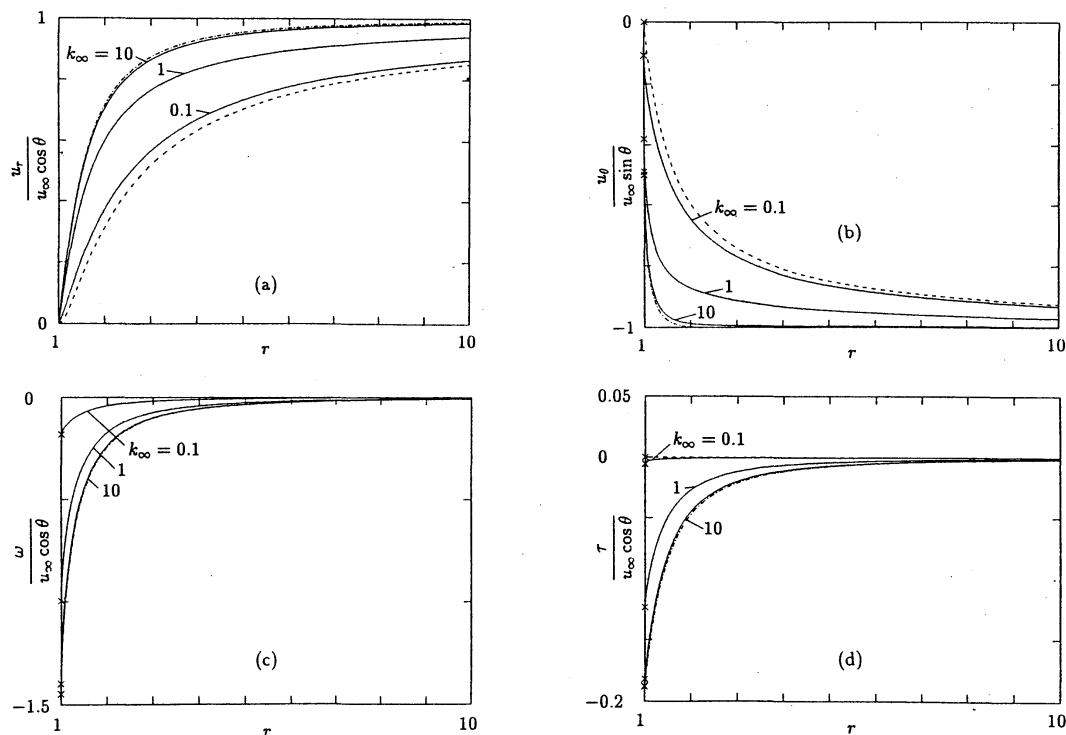
FIG. 3. The profiles of the macroscopic variables (hard sphere). (a) $u_r/u_\infty \cos\theta$ vs r, (b) $u_\theta/u_\infty \sin\theta$ vs r, (c) $\omega/u_\infty \cos\theta$ vs r, and (d) $\tau/u_\infty \cos\theta$ vs r. Here, ———— indicates the present numerical result, ----- the asymptotic solution (26a)-(26d) with $k_\infty = 0$, and —·—·— the free molecular flow ($k_\infty = \infty$). The $\times$ indicates the value at $r = 1$.
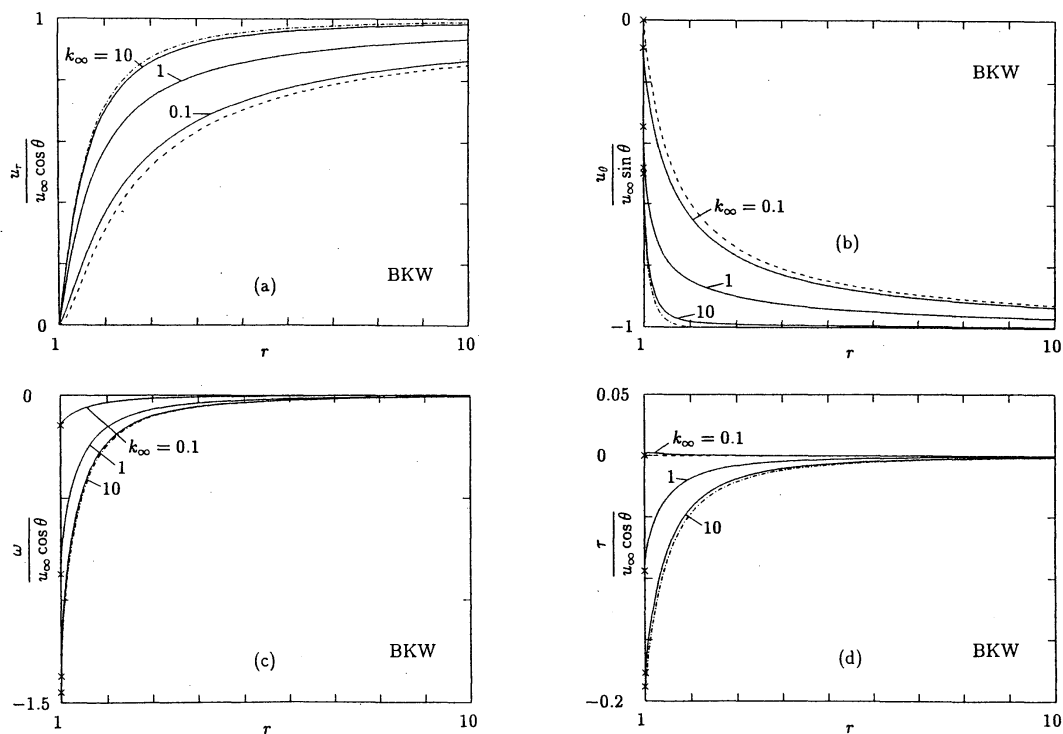
FIG. 4. The profiles of the macroscopic variables (BKW). (a) $u_r/u_\infty \cos\theta$ vs r, (b) $u_\theta/u_\infty \sin\theta$ vs r, (c) $\omega/u_\infty \cos\theta$ vs r, and (d) $\tau/u_\infty \cos\theta$ vs r. Here, ———— indicates the present numerical result, - - - - - the asymptotic solution (26a)-(26d) with $k_\infty = 0$, and — — — the free molecular flow ($k_\infty = \infty$). The $\times$ indicates the value at $r = 1$. The conversion (58) of k_∞ is not made here.
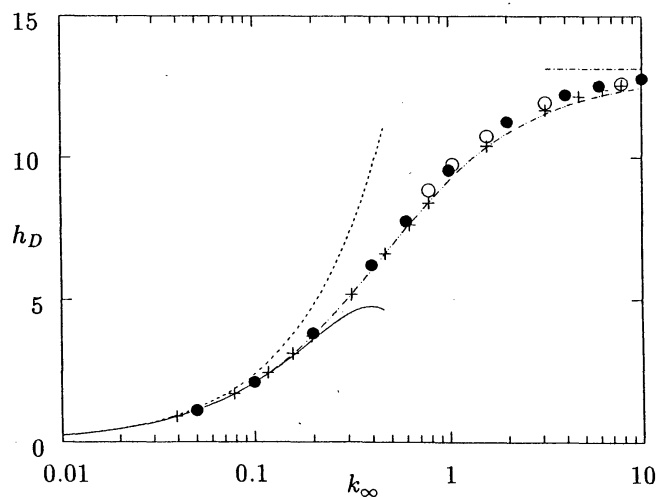
FIG. 5. The drag on the sphere: h_D vs k_∞. The drag F_i is given by $F_i = p_\infty L^2 (2RT_\infty)^{-1/2} U_i h_D$ [Eq. (56)]. Here, ● indicates the present result for hard-sphere molecules, + the present result for the BKW model, ○ the result by kernel expansion method (Ref. 24), — — — the empirical formula by Millikan (Ref. 3), ———— the asymptotic result for small k_∞ [Eq. (57b)], - - - - - the Stokes drag [the first-order term in k_∞ of Eq. (57b)], and — — — the result for the free molecular flow [Eq. (57a)].
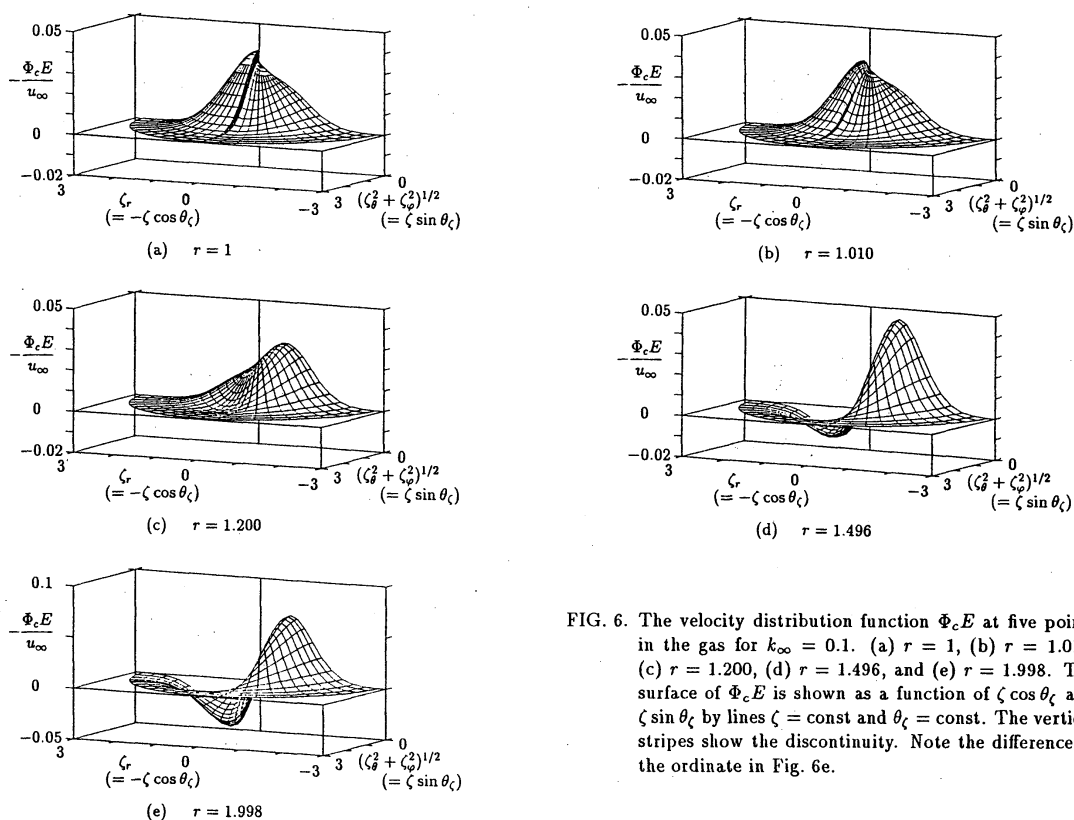
FIG. 6. The velocity distribution function $\Phi_c E$ at five points in the gas for $k_\infty = 0.1$. (a) $r = 1$, (b) $r = 1.010$, (c) $r = 1.200$, (d) $r = 1.496$, and (e) $r = 1.998$. The surface of $\Phi_c E$ is shown as a function of $\zeta \cos \theta_\zeta$ and $\zeta \sin \theta_\zeta$ by lines $\zeta = \text{const}$ and $\theta_\zeta = \text{const}$. The vertical stripes show the discontinuity. Note the difference of the ordinate in Fig. 6e.
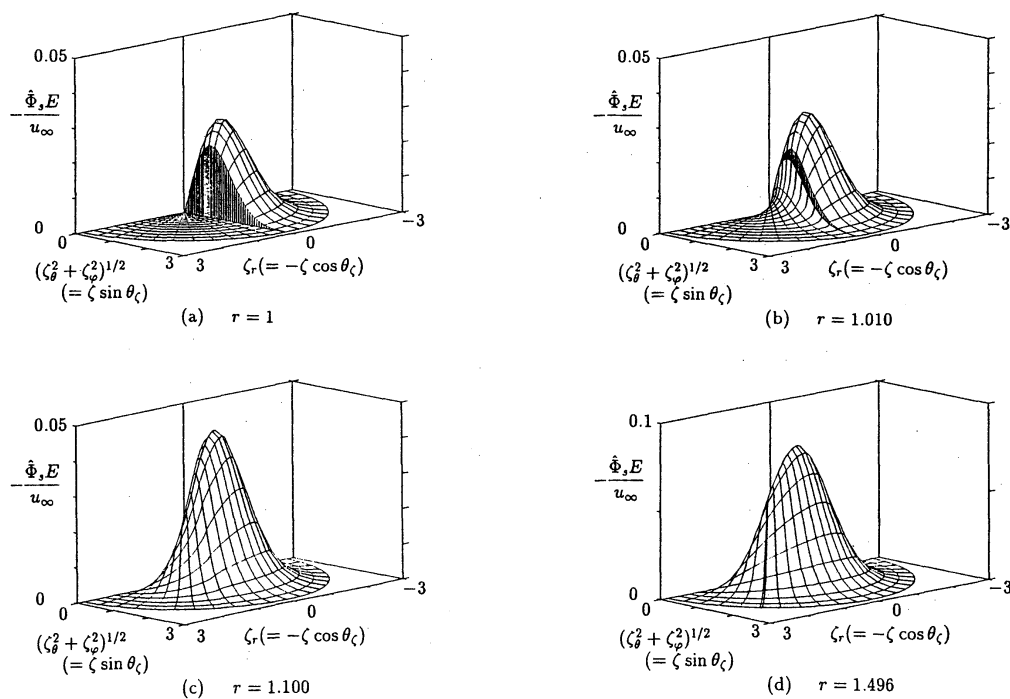
FIG. 7. The velocity distribution function $\hat{\Phi}_s E$ at four points in the gas for $k_\infty = 0.1$. (a) $r = 1$, (b) $r = 1.010$, (c) $r = 1.100$, and (d) $r = 1.496$. The surface of $\hat{\Phi}_s E$ is shown as a function of $\zeta \cos \theta_\zeta$ and $\zeta \sin \theta_\zeta$ by lines $\zeta = \text{const}$ and $\theta_\zeta = \text{const}$. The vertical stripes show the discontinuity. Note the difference of the ordinate in Fig. 7d.

(a) $r = 1$

(b) $r = 1.100$

(c) $r = 1.498$
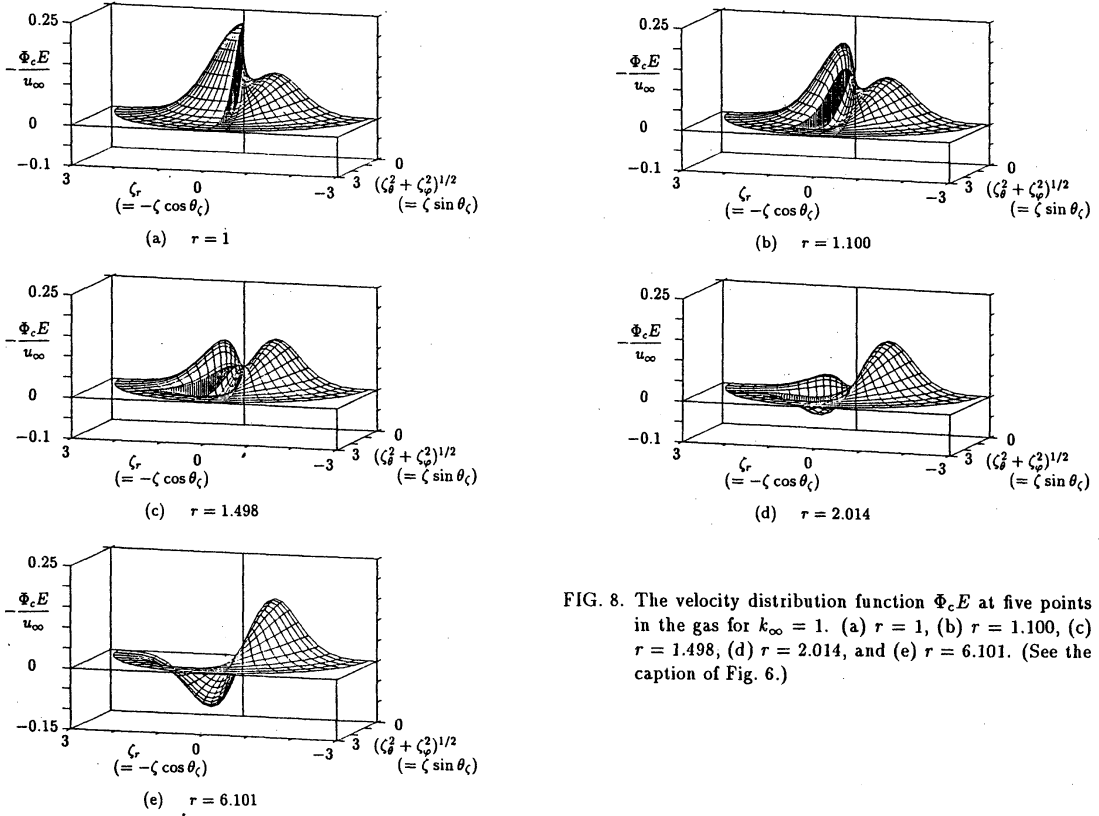
(d) $r = 2.014$

(e) $r = 6.101$

FIG. 8. The velocity distribution function $\Phi_c E$ at five points in the gas for $k_\infty = 1$. (a) $r = 1$, (b) $r = 1.100$, (c) $r = 1.498$, (d) $r = 2.014$, and (e) $r = 6.101$. (See the caption of Fig. 6.)

(a) $r = 1$

(b) $r = 1.100$
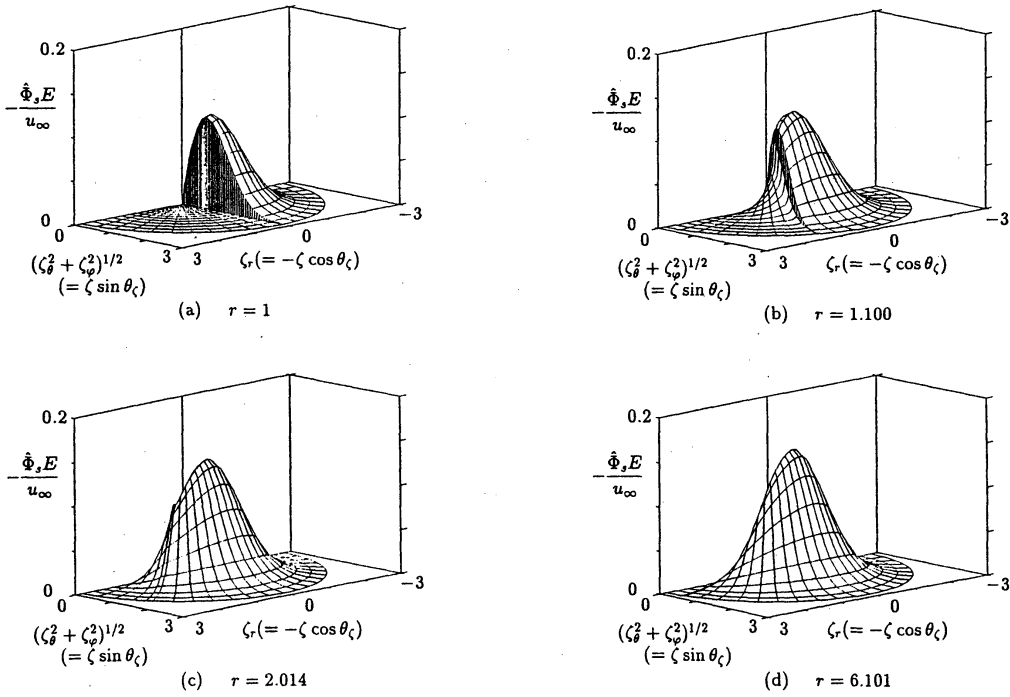
(c) $r = 2.014$

(d) $r = 6.101$

FIG. 9. The velocity distribution function $\hat{\Phi}_s E$ at four points in the gas for $k_\infty = 1$. (a) $r = 1$, (b) $r = 1.100$, (c) $r = 2.014$, and (d) $r = 6.101$. (See the caption of Fig. 7.)
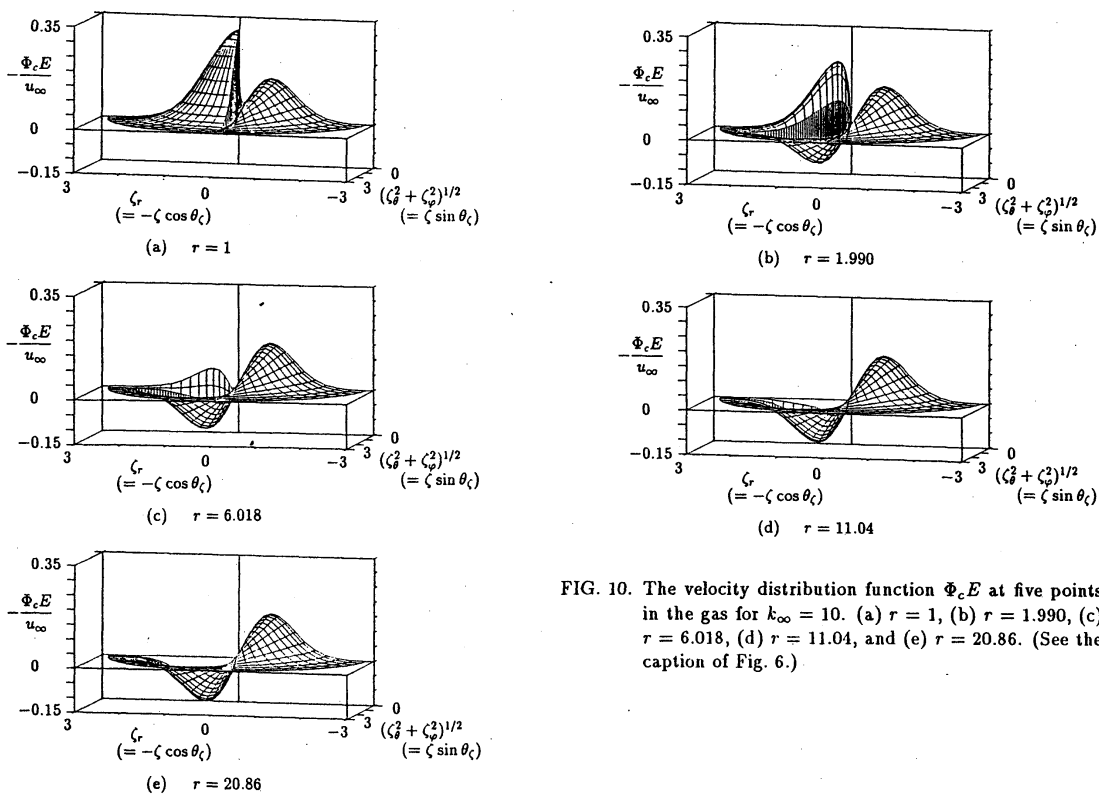
FIG. 10. The velocity distribution function $\Phi_c E$ at five points in the gas for $k_\infty = 10$. (a) $r = 1$, (b) $r = 1.990$, (c) $r = 6.018$, (d) $r = 11.04$, and (e) $r = 20.86$. (See the caption of Fig. 6.)
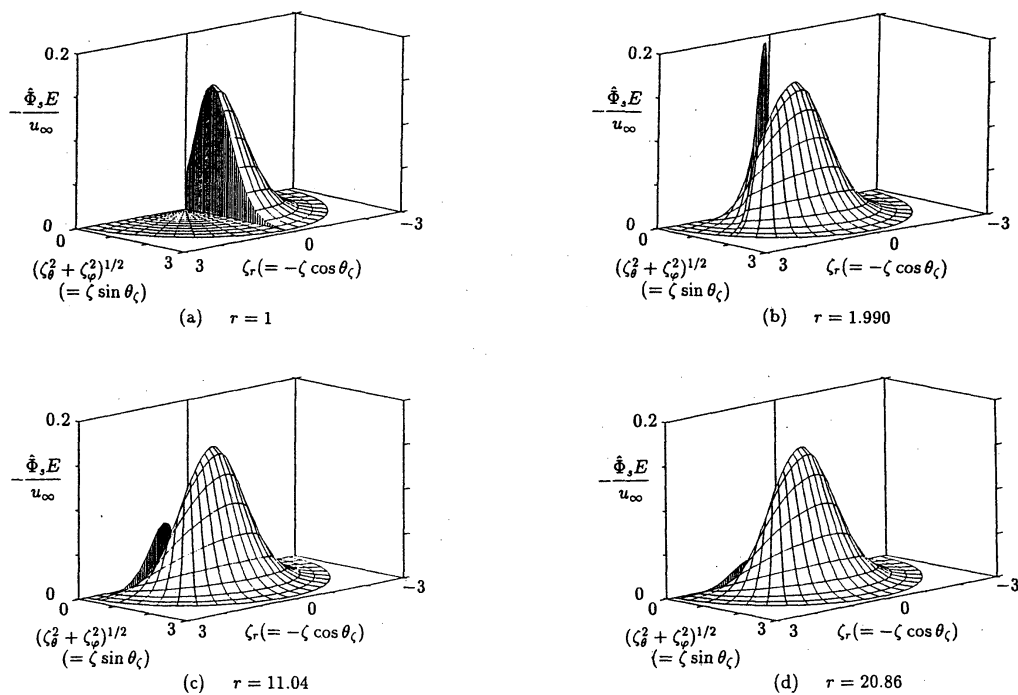
FIG. 11. The velocity distribution function $\hat{\Phi}_s E$ at four points in the gas for $k_\infty = 10$. (a) $r = 1$, (b) $r = 1.990$, (c) $r = 11.04$, and (d) $r = 20.86$. (See the caption of Fig. 7.)
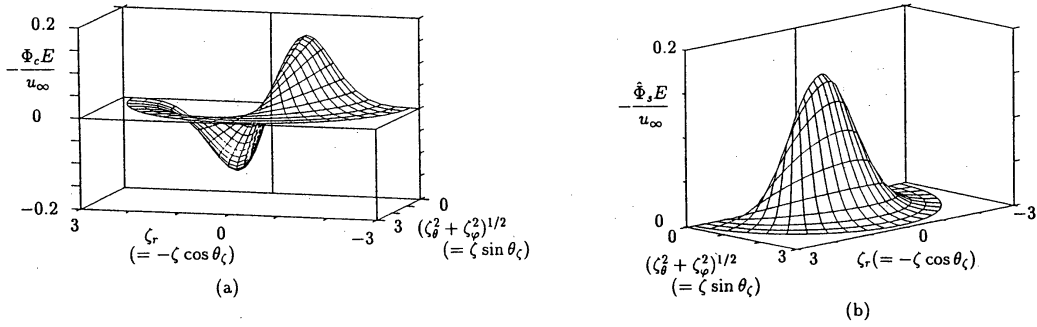
FIG. 12. The velocity distribution functions $\Phi_c E$ and $\widehat{\Phi}_s E$ in the uniform flow at infinity. (a) $\Phi_c E$ and (b) $\widehat{\Phi}_s E$. (common to all k_∞)
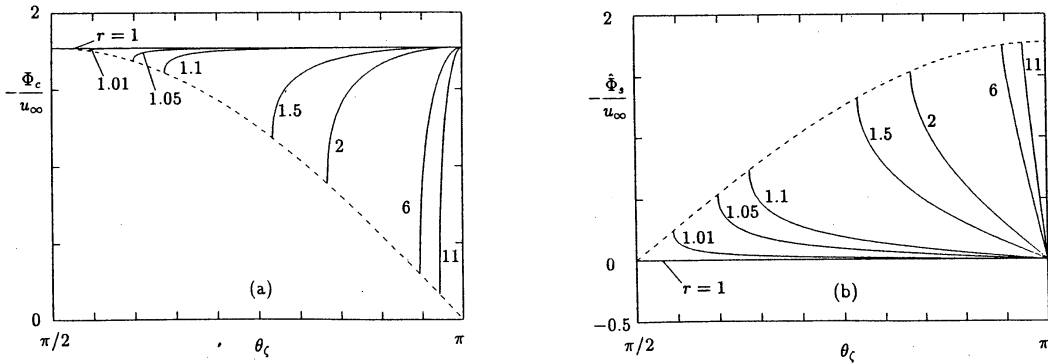
FIG. 13. The velocity distribution functions Φ_c and $\widehat{\Phi}_s$ for $\pi - \text{Arcsin}(1/r) < \theta_\zeta \leq \pi$ (the molecules coming directly from the sphere) in the free molecular flow [Eqs. (23) and (24)]. (a) Φ_c and (b) $\widehat{\Phi}_s$.
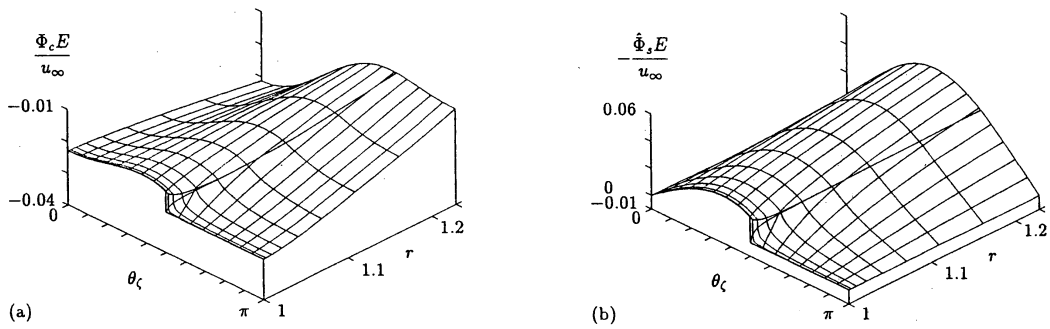
FIG. 14. The velocity distribution functions $\Phi_c E$ and $\widehat{\Phi}_s E$ at $\zeta = 0.556$ for $k_\infty = 0.1$. (a) $\Phi_c E$ and (b) $\widehat{\Phi}_s E$. The surfaces of $\Phi_c E$ and $\widehat{\Phi}_s E$ are shown as functions of r and θ_ζ by lines $r = \text{const}$ and $\theta_\zeta = \text{const}$. The vertical lines show the discontinuity. The invisible lines behind other parts are shown by dashed lines.
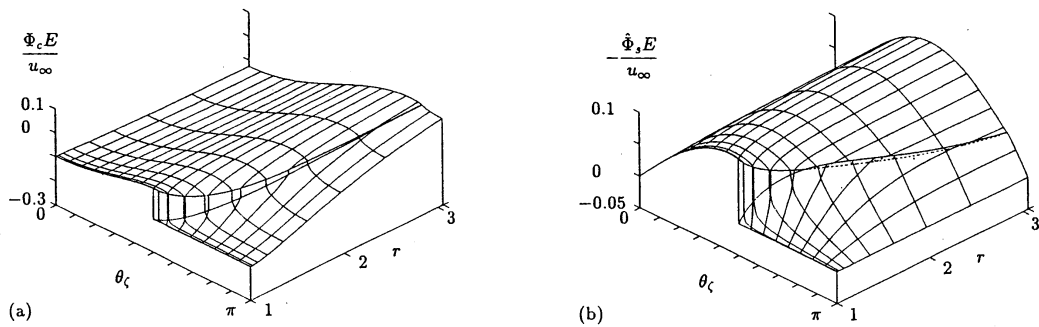
FIG. 15. The velocity distribution functions $\Phi_c E$ and $\widehat{\Phi}_s E$ at $\zeta = 0.556$ for $k_\infty = 1$. (a) $\Phi_c E$ and (b) $\widehat{\Phi}_s E$. (See the caption of Fig. 14.)
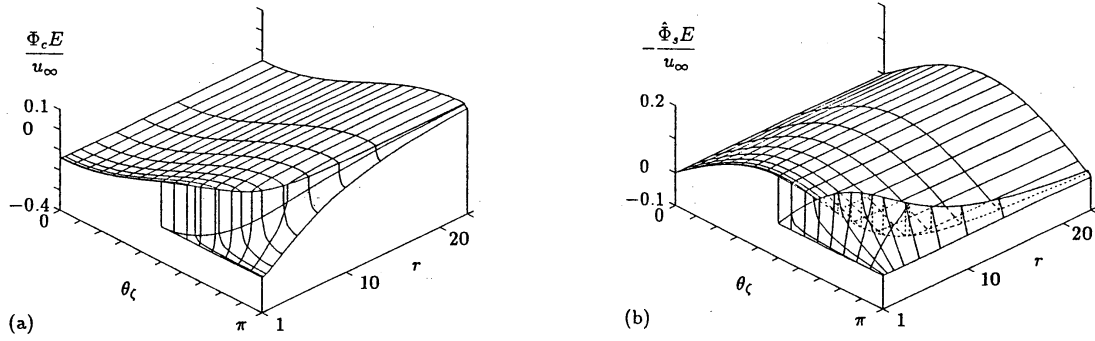
FIG. 16. The velocity distribution functions $\Phi_c E$ and $\widehat{\Phi}_s E$ at $\zeta = 0.556$ for $k_\infty = 10$. (a) $\Phi_c E$ and (b) $\widehat{\Phi}_s E$. (See the caption of Fig. 14.)
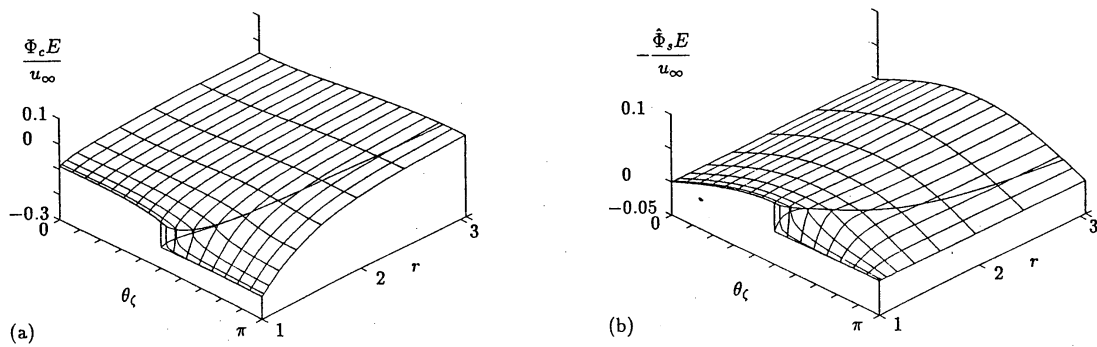
FIG. 17. The velocity distribution functions $\Phi_c E$ and $\widehat{\Phi}_s E$ at $\zeta = 0.139$ for $k_\infty = 1$. (a) $\Phi_c E$ and (b) $\widehat{\Phi}_s E$. (See the caption of Fig. 14.)
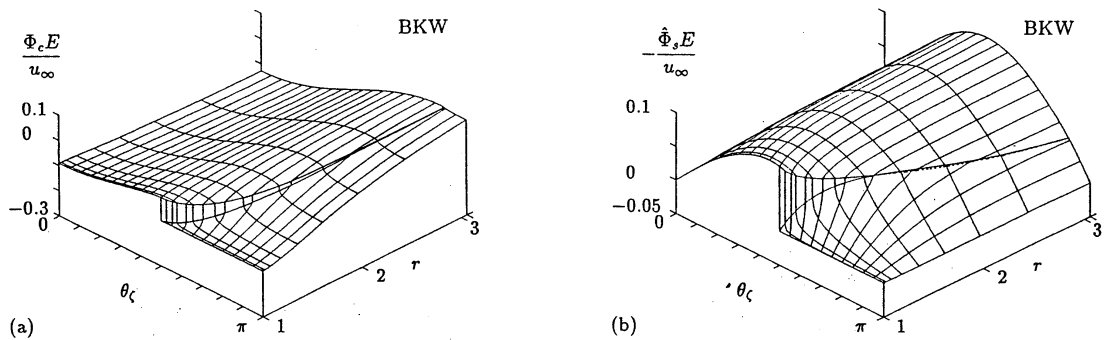
FIG. 18. The distribution functions $\Phi_c E$ and $\widehat{\Phi}_s E$ for the BKW equation at $\zeta = 0.667$ for $k_\infty = 1$, which corresponds to Fig. 15 (hard sphere). (a) $\Phi_c E$ and (b) $\widehat{\Phi}_s E$. (See the caption of Fig. 14.) The conversion (58) of k_∞ is not made here. Note the difference of the value ζ from that in Fig. 15.